Department of Precision and Microsystems Engineering

Predictive Capabilities of a Simplified 2D Model for Quasi-Zero-Stiffness Beam-Node Metamaterials

Duran Manshanden

Report no : 2026.004
Coach : Dr. F.G.J. Broeren
Specialisation : Mechatronic System Design (MSD)
Type of report : Master Thesis
Date : 28 January 2026

Delft University of Technology

MASTER THESIS

Precision and Microsystems Engineering

Predictive Capabilities of a Simplified 2D Model for Quasi-Zero-Stiffness Beam-Node Metamaterials

---

Author:
ing. Duran Manshanden

Supervisor:
Dr. F.G.J. Broeren

January 21, 2026

Abstract

Mechanical vibrations can reduce the performance of precision systems, motivating the development of adaptable vibration isolation solutions. This thesis investigates a beam-node metamaterial, designed to exhibit quasi-zero-stiffness behavior through geometric nonlinearity. A simplified two-dimensional model consisting of horizontal, vertical, and diagonal slender beams is optimized using a genetic algorithm to address discrete design variables and nonlinear structural response. The optimized design is manufactured and experimentally evaluated through static compression and dynamic vibration tests. Numerical simulations are compared with experimental results to assess the predictive accuracy of the model. The results show that the simplified beam-node model captures the key static behavior of a single unit cell. While deviations occur for small metamaterials due to boundary effects and material-related phenomena. Furthermore, deviations in the dynamic behavior of small metamaterials are identified, and the source of this behavior is explained through additional testing. This study shows that a simple beam-node metamaterial combined with an efficient optimization strategy is a viable approach for vibration isolation solutions, laying the foundation for its experimental realization.

Contents

1 Introduction

Mechanical vibrations often occur in moving mechanical structures such as robotic arms or 3D printers, these mechanical vibrations can influence the surrounding of these structures. The overall performance of these mechanical structures is reduced when large external vibrations are present. Therefore, having multiple of these structures in proximity could result in performance reduction. Low frequency vibrations occur every day through normal processes such as a car or tram driving by. These low frequency vibrations could disrupt sensitive testing and manufacturing processes. To mitigate all disruptive vibrations, various linear vibration isolation structures have been designed.[1–3]

These linear vibration isolation structures isolate specific frequency bands and generally have a large and complex shape. Moreover, these existing structures are designed for one specific range of frequencies, resulting in different designs for different frequency bands. In these cases, an easily tunable vibration isolation design would be preferred.[4–6]

An alternative to such large and complex isolation structures is the use of emerging properties in specially designed metamaterials. Metamaterials are materials designed with a small cellular structure to enhance specific material properties.[7–9] With specifically designed unit cells, at a small scale, the total structure could assume the properties of the individual unit cells.

One of the approaches used in the literature [3, 6, 10–15] to obtain a vibration isolation metamaterial consists of combining a component with a positive stiffness and a component with a negative stiffness. When these positive and negative stiffness parts are used in the same structure, a quasi-zero stiffness (QZS) region is obtained, which can be recognized by the horizontal section in a force-displacement graph. Within a QZS region, the structure is able to move up and down without using energy. Therefore, the structure should be able to isolate vibrations over a broad range of frequencies when the force corresponding to the QZS region is applied. A problem when attempting to model such a structure is the requirement to use nonlinearity in the model, resulting in expensive simulations. The nonlinearity is necessary to obtain near-zero stiffness. To mitigate the calculation costs, a specific 2D beam-node model has been investigated during this thesis research project. A beam-node model is a model consisting of one-dimensional slender beams in a 2D kinematic space. The design during this project has been a combination of horizontal, vertical, and diagonal slender beams. This combination of beams enables geometric nonlinearity through displacement coupling while maintaining a simple and computationally efficient beam-node model. Therefore, the nonlinear behavior should originate from the geometry and not the material.[16–19]

The aim of this project is to identify the vibration isolation behavior of an optimized simple beam-node structure. At the end of this project, the following main research question will be answered: "To what extent does a simplified 2D simulation model of a beam-node metamaterial designed for quasi-zero stiffness accurately predict its experimentally observed static and dynamic behaviors?"

To answer this question, firstly, a simple beam-node structure has been optimized through a process of removing and adding beams. The starting structure is based on a set of horizontal, vertical, and diagonal beams. Due to the nonlinearity property in these slender beams, a QZS region can be obtained. Secondly, physical properties of the optimized design has been obtained through static compression tests and dynamic vibration tests.

The focus of this thesis project is to identify the static and dynamic behavior of an optimized design. The optimization process is to obtain a design with a QZS region that can be tested. The objective is to obtain a working design, not the absolute optimal design. In addition, due to time constraints, only one material has been used to evaluate the sample behavior.

This paper is structured as follows. The methodology will be discussed in chapter 2. This includes the optimization approach, how the model is constructed, and what variables are used. In addition, chapter 2 contains a discussion on the production of the test samples and details related to the static compression tests and dynamic vibration tests. Chapter 3 presents the results from all the tests and their corresponding simulations. These results will be interpreted and discussed in chapter 4, followed by a conclusion in chapter 5.

2 Methodology

This chapter outlines the methodology followed throughout this research project. The methodology is divided into four sections, beginning with the optimization approach. This section explains the objective of the optimization process and the method used to achieve it. Furthermore, the underlying assumptions and limitations are described to ensure a correct interpretation of the resulting data.

The second section focuses on the test specimen, including its design, modeling, and manufacturing procedure.

The third section covers the static compression tests that were conducted. Details are provided regarding the testing equipment, its operational constraints, and the test procedures. Additionally, a discussion follows on the selection of test configurations and corresponding specimens.

The fourth and final section presents the dynamic vibration testing methodology. Similar to the static testing section, it describes the purpose of these tests, the experimental setup, and the procedures used to evaluate the dynamic response of the samples.

2.1 Optimization approach

The simulations are performed using the software COMSOL Multiphysics LiveLink for MATLAB.[20, 21] COMSOL handles the beam-node structural model, while MATLAB is used for result extraction, geometry modification, and the execution of the optimization algorithm. The 2D beam-node model is based on a one dimensional slender beam formulation in a two-dimensional kinematic space. The beam-node model is selected due to its significantly higher computational efficiency compared to full 3D solid simulations. [22] Additionally, its parametric nature allows straightforward scaling of the structure, for example scaling a 3x3 configuration to a 5x5 configuration, thus enabling exploration of more design variations during optimization.

A genetic algorithm (GA) was selected to handle the discrete beam-removal-design variables and the nonlinear evaluation of the structural response. Its gradient-free nature enables robust exploration of the design space and supports the identification of an experimentally viable structure.[23]

2.1.1 The optimization model

The baseline model is defined by a square grid of nodes connected by slender beams. The structure size is specified by the number of nodes per row and column; due to symmetry, only odd values are used as that ensures there is always a node in the center of the structure. For example, a size of 5 corresponds to 5 nodes per row and column, with 4 horizontal and 4 vertical beams in each direction. Diagonal beams are included between all neighboring nodes. The beam length defines the spacing between nodes and represents both the planar spacing and the theoretical depth of the structure. An example of a 5x5 configuration is shown in Figure 1.

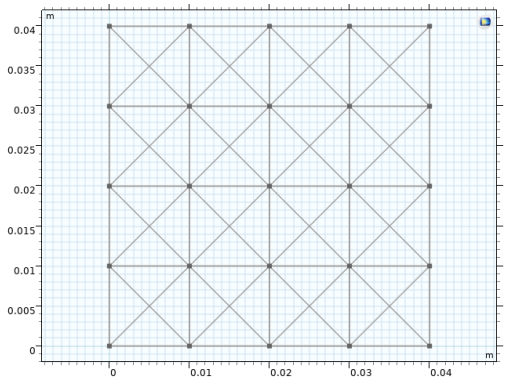

Figure 1: Full 5x5 structure with horizontal and vertical beam lengths of 1cm

Beams in this grid can be switched on or off during optimization. This binary formulation constrains the search space, making the problem discrete. Although this limits the absolute solution space, increasing the grid size compensates by introducing more degrees of freedom. This structure allows for simple manufacturing, modeling, and analyzing, while the anticipated buckling of slender beams is expected to induce local negative stiffness, thereby supporting the creation of a QZS region.[3, 6, 24]

Two design configurations were investigated throughout this work: a single unit cell design and a periodic metamaterial design. The metamaterial configuration uses the same beam-node layout as the single unit cell model, but with additional periodic boundary conditions (PBCs). Studying both cases enables assessment of the influence of PBCs when optimizing for a QZS region. Each configuration has been analyzed separately to obtain a complete understanding of its structural behavior. For the metamaterial configuration, PBCs are applied to represent a theoretically infinite repetition in both horizontal and vertical directions. In practice, manufactured specimens will always exhibit boundary effects, which are not captured by these idealized conditions.[25]

The beam-node model in COMSOL follows the assumption of 'slender beams' [22], meaning that the length of the beam is significantly larger than the cross sectional area. As a result, the model assumes only one dimensional stress distributions and no in-plane bending. Additionally, certain beams at the model boundaries remain permanently activated in the metamaterial case to avoid double-thickness connections in the periodic layout. These constraints reduce the number of feasible designs but ensure physical manufacturability. A key limitation of the beam-node approach is the absence of contact modeling between beams that are not directly connected.[22] At large deformations, physical interference between beams is inevitable in reality, leading to rapid stiffness growth. Similarly, material and geometric imperfections in manufactured samples are ignored and may have a pronounced impact due to the small beam thickness. The simulations are provided with a linear elastic isotropic material model, where the linear material properties are obtained with ISO 527-1 tensile tests.

In this optimization process, several settings are available to influence the end results. The first and most visible setting is the size, which is defined as the number of points in the rows and the columns. Larger size results in more beams and therefore more possible configurations of the

beam-node model. During this project a size of 5 is implemented. With this size, the calculation costs are minimal while maintaining enough possible structures. In addition, this size provides the possibility for the beam parameters to be chosen such that the buckling is visible while the 'slender beam' assumption is still valid with the minimal thickness availible.

The length is defined as the length of a single beam between two nodes. The total length and width of the design will be the length multiplied by the size minus one. Changing the length could have significant influence on the bending property of the beams due to the length-thickness ratio. In addition, the length is the theoretical depth in the model. The depth of the model is relatively large to ensure there is no in-plane bending. Increasing the depth of the structure has no influence on the shape of the force-displacement curve. The only effect is a small increase of force for all displacement values.
The thickness is defined as the theoretical thickness of each beam. Increasing the thickness has a similar effect as increasing the depth of the structure: the shape of the graph remains unaltered, however the force values are all lifted equally. This property can be useful to relocate the flat plateau to a specific force value.

2.1.2 The optimization process

The optimization program is designed where a structure, consisting of square thin beams in a n by n grid including diagonals (see Figure 1), is optimized to obtain a force-displacement curve with a flat plateau (zero stiffness). The two main goals for this curve is to have a near horizontal section which is as long as possible, while it being as flat as possible, see Figure 2. A column vector is used in this model to describe all the beams, where each row corresponds to a beam. The value in that row is either 1 or 0 (on or off) in a binary style. During the optimization process this vector is used as the variable to obtain new geometries. The optimization program starts with a base model, which is the starting structure. In each iteration of the GA, the objective function adjusts the geometry based on the new beam vector (the variable), calculates the force-displacement curve, and calculates the fitness based on this curve.

Table 1: Optimization settings

Setting	Value	Unit
Size	5	-
Length	0.01	meter
Thickness	0.0007	meter
Displacement of compression	0.01	meter
Step size	30	-
Closeness	0.05	-
Population size	20	-
Max Generations	10	-
Max Stall generations	5	-

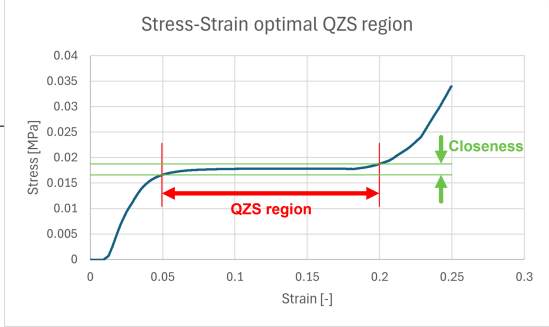

Figure 2: Example of stress-strain curve with QZS region (red) and closeness parameter (green)

There are several settings one can adjust to influence the speed, quality, and overall results of the optimization process. These settings are presented in Table 1. One notable setting is the closeness, which describes how close the curve must be to a flat optimum. An example of a large

closeness is presented in Figure 2. In addition, several GA options are available to influence the duration and size of the optimization process.

The objective function is set up as follows. For each design iteration, the force-displacement is calculated, from this, the fitness is determined. A normalized force difference is calculated for each point on this curve according to Equation 1. The normalized force values are compared against the closeness setting.

$$\Delta F = \frac{f_{i+1} - f_i}{f_i} \tag{1}$$

$$f_0 = 100 \frac{|\Delta F_{min}|}{cl} \tag{2}$$

$$f_1 = \frac{\Delta F_1}{cl} + \frac{|\Delta F_{min,\,other}|}{cl} \tag{3}$$

$$\begin{aligned} f_2 &= [flatness] + [plateau\ length] + [negativity] + [weight] \\ &= \frac{|\Delta F_{1,\,avg}|}{cl} + \frac{\frac{n-1}{n_{cl}} - 1}{\frac{n-1}{2} - 1} + \frac{|\Delta F_{1,\,neg,\,avg}|}{cl} + \frac{1}{5N} \sum_{i=1}^{N} b_i \end{aligned} \tag{4}$$

There are three options when comparing the normalized force and the closeness:

1. There are no normalized force values smaller than the closeness, then Equation 2 will be applied.
2. There is only one normalized force value smaller than the closeness, then Equation 3 is applied.
3. There are multiple normalized force values smaller than the closeness, then Equation 4 is applied.

All normalized force values outside the closeness area are denoted with ΔF_0, all normalized force values inside the closeness area are denoted with ΔF_1. The closeness value is denoted with cl. The total number of measurement points is denoted with n and the number of measurement points corresponding with a normalized force value within the closeness area is denoted with n_{cl}. The beam vector describing the geometry is denoted by b and has N elements.

There are two optimization settings that are closely correlated, which are the displacement of the compression and the number of steps. Both these settings have a large influence on the force-displacement graph. The displacement of compression influences the size of the x-axis, and the number of steps influences the distance between the calculated points. The goal of the optimization process is to find a geometry with a force-displacement curve with a flat plateau. Therefore, it is necessary to include enough displacement for the plateau to fit while keeping it as small as possible due to calculation costs. The number of steps must be large enough to obtain enough results in the fitness calculation while keeping it as small as possible due to calculation costs. At large values for the displacement, collision effects are not included in the COMSOL beam model, the compression calculated for large displacement values may not be accurate.[22]

Another setting is the closeness. This value is used in the fitness calculation by comparing it to the normalized force. The closeness defines how far the normalized force values can deviate from zero. Increasing the closeness result in a less flat plateau, however, this might be necessary when using a lower number of steps.

GA options are settings within the optimization process that can influence the optimized result. The most influential GA option is the population size. This value defines how many different different geometries are attempted for each generation.[26] Increasing the population size results in a bigger chance of the program returning the global optimum. However, a higher population size increases the calculation costs as well.
There are two situations where the optimization program ends: a maximum generation is reached or the resulting fitness does not change for several generations. Both the maximum generations and maximum stall generations are options that can be changed. Increasing the number of generations results in more time to find the optimal solution at the cost of more calculations. To ensure that the GA stops once an optimal solution is achieved, a maximum stall generations option is used. This is the amount of generations that result in the same fitness before the GA stops.

To ensure that the design can be manufactured and loaded properly, several beams are fixed and cannot be turned off during the optimization process. As a result this limits the amount of possible configurations, however, this ensures that the optimized result can always be manufactured and tested. The fixed beams are different for the two conditions (single unit cell and metamaterial) and will be discussed in their corresponding sections.

2.2 Test samples

Before experimental testing can be conducted, several test samples must be manufactured. Key decisions include the selection of the manufacturing method, the material, and the specific designs to be produced. This section discusses these decisions and their underlying motivations. Two types of experimental tests have been performed: static compression testing and dynamic vibration testing. During these tests a variety of designs helps ensure that the results are not specific to a single geometry but instead provide broader insight into the overall design strategy.

The static compression tests and the dynamic vibration tests have been carried out using the same optimized single unit cell design to enable a direct comparison between static and dynamic responses. Furthermore, a metamaterial version of this unit cell has been evaluated in the dy-

namic vibration tests to assess the influence of periodicity on the structural behavior. For the force-controlled oscillating compression tests, a different single unit cell design was used. This design includes a higher number of beams, resulting in increased stiffness, which improves the visibility of displacement shifts during cyclic loading. All test geometries are obtained using the optimization methods described earlier in this chapter.

The specimens were additively manufactured using a Fused Deposition Modeling (FDM) 3D printer with Thermoplastic Polyurethane (TPU) material. To ensure accurate representation of material behavior in the simulations, tensile tests are performed to determine the necessary mechanical properties of the printed TPU.

The numerical model is based on a one-dimensional slender-beam formulation. The most direct translation of this model into a three-dimensional physical structure is to assign a finite beam thickness and extrude the geometry accordingly. The optimized example is presented in Figure 3. This approach results in a design that is well-suited for fabrication using the FDM process.

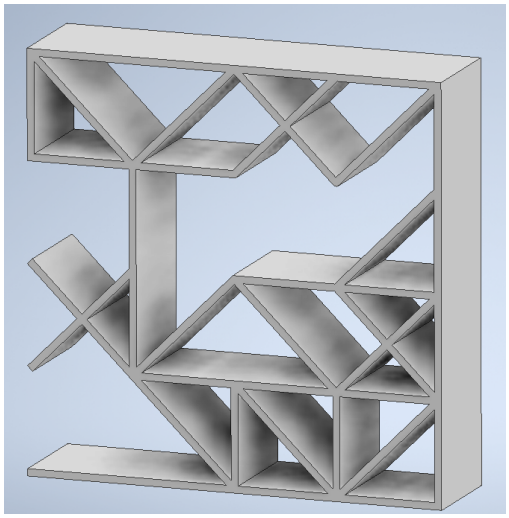

Figure 3: 3D structure of the optimized 2D model

TPU is selected as the material for manufacturing the test samples due to its mechanical properties and suitability for the intended metamaterial behavior. TPU exhibits a relatively low elastic modulus combined with high flexibility, which allows large elastic deformations without permanent deformations.[27] This is essential for realizing buckling-induced negative stiffness effects, which are a key mechanism for achieving a quasi-zero-stiffness (QZS) region.

The limitations of this manufacturing method are the size and material choice. FDM printing is size restricted by the nozzle size and the build plate size. Ideally, a metamaterial test sample much larger than 3x3 will be produced. However, this is not feasible with this manufacturing method. To ensure a loading condition where the loading force is equally distributed over the top of the sample, a design modification is added to the test sample. This modification includes a metal bar inserted above the top and underneath the bottom of the sample, as is highlighted

in red in Figure 4. In addition, thick tape is used during the static compression tests to prevent the sample from slipping sideways.

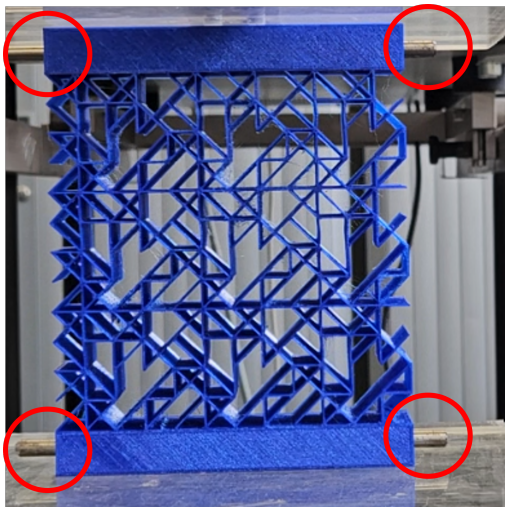

Figure 4: Compression testing configuration with design modification metal bars highlighted with red circles

2.3 Static compression test

The first tests that are performed with the samples are static compression tests using a Zwick-Roell Z005 compression machine.[28] This machine is used to compress a test sample using an input displacement while measuring the time and force. The goal of this project is to obtain a zero stiffness region in the force-displacement graph. Within the QZS region, it is possible that for one force value multiple displacement values could occur. As a result, the input setting of the compression test must be the displacement. A force-displacement graph can be produced with the input displacement and the force output. Based on the geometry of the test sample, the force-displacement graph can be converted to a stress-strain graph, which is particularly useful in comparing different-sized samples.

For the single unit cell sample the maximum compression displacement is set to 10mm, which is equal to one column length (L). Higher displacements will definitely result in clashes which are not included in the model. Moreover, the 3x3 metamaterial has been compressed three times as far to ensure an equal strain. In addition, all samples have been compressed at least three consecutive times to ensure the material is settled and a constant hysteresis loop is obtained. All the test samples have been placed between two large compression blocks, which provide an equally distributed force on the full surface area. In addition, several samples have been placed between thick tape at the sides to reduce slipping. This tape provides a horizontal force purely to prevent slipping, it does not influence the vertical force-displacement. An example of a clamped sample is presented in Figure 5.

Various samples have been tested. Firstly, a single unit cell sample has been tested, which will be used as a reference to confirm the accuracy of the model. In addition, a 3x3 metamaterial sample

has been tested to identify the properties which has been used in the dynamic vibration tests. Moreover, these two test results are used to identify the influence of the PBCs and to inspect their general behavior. In addition, a sample with only row boundary conditions (1x3 metamaterial, Figure 12) and a sample with only column boundary conditions (3x1 metamaterial, Figure 14) have been tested to identify which boundary conditions have more influence on the total 3x3 metamaterial behavior. To conclude, a force-oscillating compression test has been performed on a 3x3 metamaterial to identify a displacement shift phenomenon, which will be discussed during the vibration test results. During this specific test, the force is the input of the compression. The sample whas been compressed between two predefined force values for multiple cycles. For this specific test a sample with higher stiffness is required to better observe the displacement shift, therefore, this test has been done using a different sample than the remainder of the tests.

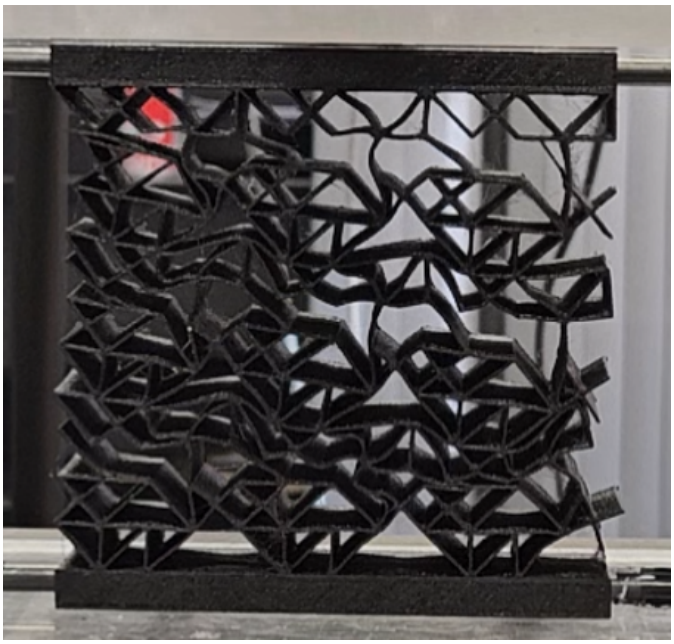

Figure 5: Static compression test setup with a metamaterial test sample

2.4 Dynamic vibration test

The static compression test described in section 2.3 can provide a good understanding of the static behavior of the test samples. However, to identify the dynamic behavior of the test samples, several vibration tests has been executed. During the vibration test the samples were placed in a shaker setup as presented in Figure 6. The object labeled 'A' is the Tira TV51110 shaker [29], this is the origin of the vibrations forced upon the test sample. The object labeled 'B' represents the test sample, and the object labeled 'C' is the weight that is forced upon the test sample. The distances to the top and the bottom of the sample from fixed reference points are independently measured using two laser displacement sensors with a range of 200mm and an error of 0.2 micrometers. These measurements were used to obtain a transmittance-frequency plot.

During the testing process the test sample was clamped using a 3D printed fit. The loading weight were spread out over the top of the sample due to this clamping. Similarly, the input

vibrations were applied to the center of the test sample. The weights used in this test setup were small lead balls, this ensured an equal loading area to prevent any unbalanced deformations.

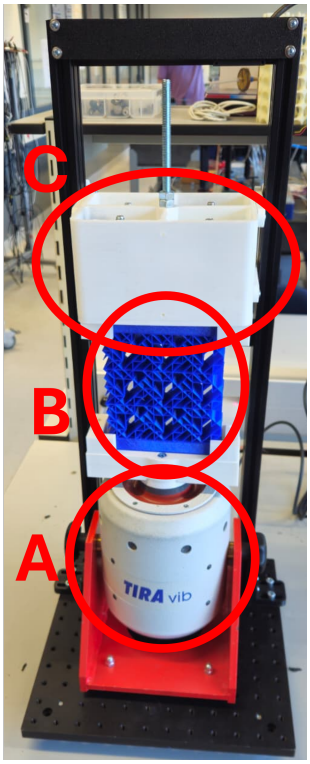

Figure 6: Dynamic vibration test setup with the Tira TV51110 (A), the test sample (B), and the loading mass (C)

The goal of performing vibration tests was to identify when the sample exhibit's vibration isolation and if the behavior of the test sample corresponds to the predicted behavior based on the static tests.

The transmittance-frequency graph was obtained by performing a frequency sweep on the preloaded test sample. The load was fixed and will not change during the frequency sweep. Once loaded, a frequency sweep from 1Hz to 20Hz was performed, where each frequency was measured for 120 seconds.

3 Results

This chapter provides the results from the optimization process, static compression tests, and dynamic vibration tests. First, the results of the single unit cell model and compression tests are provided. Second, the results of static compression tests of the metamaterial are provided. In this section, the effects of implementing a metamaterial compared to a single unit cell will be visualized. Then, the results from dynamic vibration tests of the metamaterial are presented. These results are then compared to simple mass-spring simulations to verify the observed behavior. Finally, results from force-induced static compression tests are presented.

With the input values presented in Table 1, the optimization process has found an optimal structure that is presented in Figure 8. The optimization process has stopped after 8 generations due to the maximum stall generation condition. The fitness corresponding to this optimal design is 0.107.

3.1 Displacement-induced static compression tests

In this section, the results of the displacement-induced static compression tests of both single unit cell and metamaterial are provided. The results of these tests are provided in several stress-strain curves due to the ability to compare different size samples. Firstly, the results of the single unit cell will be provided, followed by the results of the metamaterial samples.

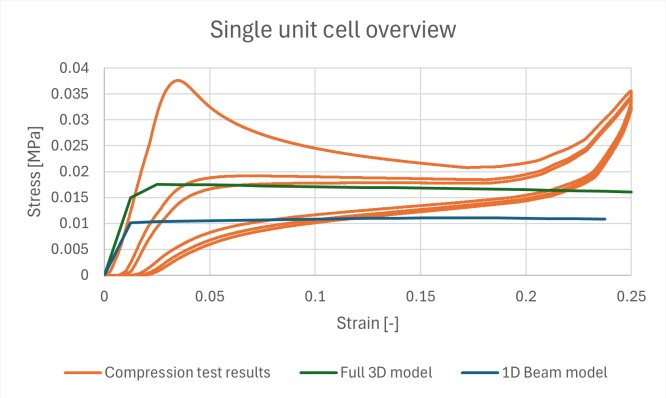

Figure 7: Single unit cell: Model 2D, model 3D, and compression test

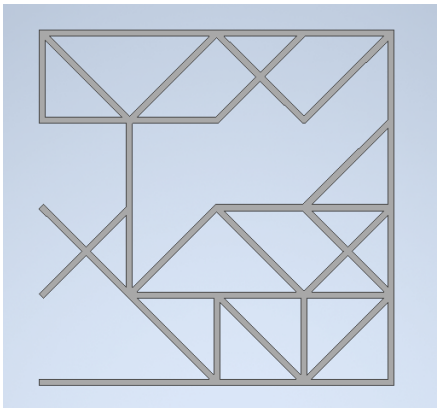

Figure 8: Single unit cell structure

Figure 7 presents the results of the single unit cell. In this graph, the displacement-induced compression test results of three compression cycles, the results of the optimized 2D beam model, and the results of a full 3D model are provided. The compression test results present a positive stiffness for low and high strain values, with a QZS region between these strain values. In addition, a change in shape for different compression cycles can be seen, with a trend towards a limit cycle behavior.

Both the models present a similar positive stiffness behavior for low strain values, following with a QZS region. However, there is no change to positive stiffness at high strain values in both models, while this does occur during the test. This positive stiffness is caused by the separate

beams colliding in each other, where the model does not include these clashes.

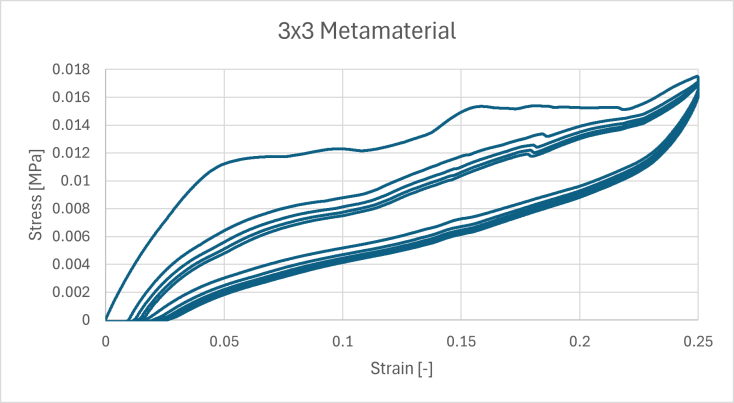

Figure 9: Stress-strain curve of 3x3 metamaterial

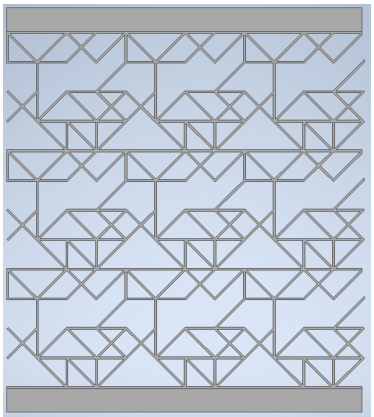

Figure 10: 3x3 metamaterial structure

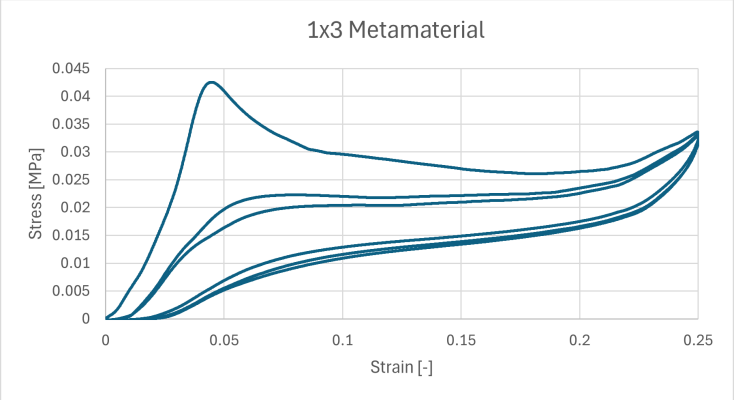

Figure 11: Stress-strain curve of 1x3 metamaterial

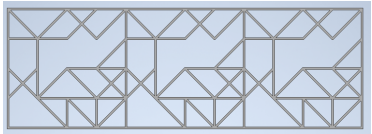

Figure 12: 1x3 metamaterial structure

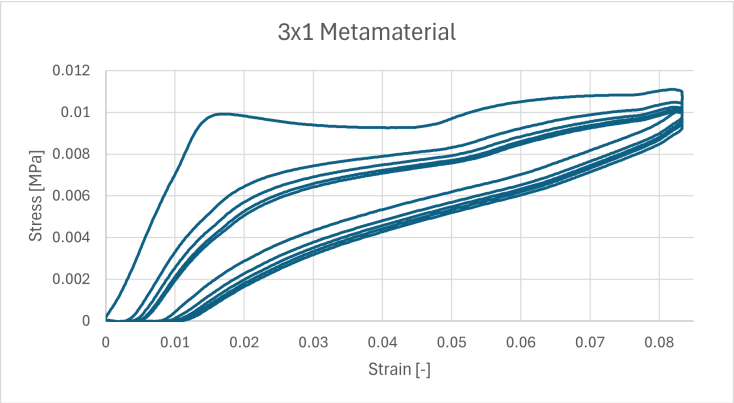

Figure 13: Stress-strain curve of 3x1 metamaterial

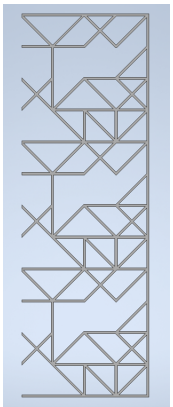

Figure 14: 3x1 metamaterial structure

The interaction between the separate unit cells is essential to properly constrain the model. Therefore, four separate samples are produced and tested. One sample for a single unit cell (Figure 7), one sample for a full three by three metamaterial (Figure 9), one sample contains three unit cells in one row (Figure 11), the other sample contains three unit cells in one column (Figure 13). The results from compression testing of these samples could indicate the effects of the boundary conditions on the overall performance. In addition, the results of the row and column samples are compared to the metamaterial sample to identify the effects of combining multiple unit cells.

The predicted stress-strain curve of the 3x3 metamaterial is similar to the single unit cell. However, this predicted behavior is not what is observed from Figure 9. Instead, a relative linear limit cycle is presented, which indicates similar behavior to a spring. However, when inspecting the limit cycle, a difference in stiffness can be seen between several strain sections. For example, a relative large stiffness change occurs around 0.1 strain, and another around 0.17 strain. These sudden changes in stiffness are most likely caused by different unit cells collapsing separately.

The stress-strain curve of the row-constrained test sample (3x1 metamaterial, Figure 11) is found to be similar to the stress-strain curve of the single unit cell sample (Figure 7). For example, an initial peak during the first compression and a zero stiffness region between the strain values of 0.07 and 0.17.

The column constrained test sample (Figure 13) is compressed for a total of 10mm, which is exactly the same length as the row constrained test sample. As a result, the range of strain are different for these two tests. The stress-strain curve of the column constrained test indicates that there is no QZS region. In addition, around the strain of 0.05 a relatively large change in stiffness occurs, which is indicated by the sudden change in slope of the curve.

When comparing the single unit cell sample and the row constrained sample, in both graphs a clear QZS region can be observed in combination with an initial stress peak for low strain values.

The differences between these two graphs is the stiffness during the positive stiffness regions at low and high strain values. The stiffness is higher for the single unit cell compared to the 1x3 metamaterial.

3.2 Dynamic vibration tests

The next set of results are obtained with the dynamic vibration tests. During these tests, the 3x3 metamaterial sample is placed in the shaker setup, described in the previous chapter, and shaken using a frequency sweep at a range of loads. The results of three loading setups (20N, 25N, and 30N) are presented in Figure 15.

The row constrained compression test indicated a QZS region around a stress level of 20kPa, which is translated to a loading force of 25N. In addition, the column constrained compression test indicated a significant decrease in stiffness between the stress levels of 6kPa and 8kPa, which is translated to a loading force between 8N and 10N. To account for the additional surface area of the 3x3 metamaterial sample, these forces must be multiplied by three resulting in a loading force between 24N and 30N. In conclusion, three applied loading force values are chosen which fall within the range of the obtained QZS region and the significant stiffness decrease region.

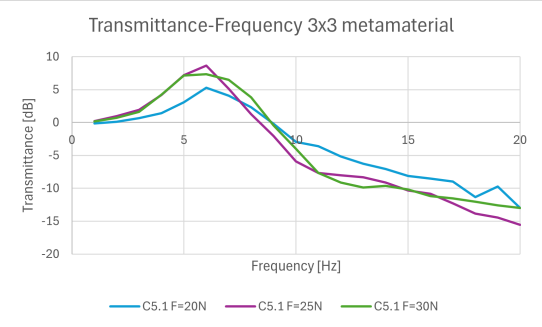

Figure 15: Transmittance-Frequency graph of 20N, 25N, and 30N

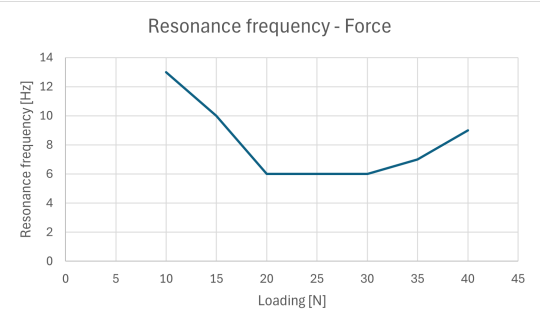

Figure 16: Resonance frequency-Loading graph

From the loading force sweep, it is observed that the applied force is related to the resonance peak frequency. Moreover, a lower resonance peak frequency results in better isolation properties. Figure 16 presents a resonance frequency-force graph with every 5N a new data point from the vibration experiments of the 3x3 metamaterial sample. From this graph it can be seen that there is a loading force range where the optimal resonance peak is observed. The expected behavior would be very similar; during the first and last phases with low and high loading forces, a relatively large stiffness is expected and therefore a higher resonance frequency. During the middle phase where QZS occurs a relatively low stiffness is expected with minimal resonance frequency. Due to this graph having a rough resolution, where every 5N a new datapoint is observed, the minimal resonance frequency is spread out over three data points instead of having one optimal resonance frequency datapoint.

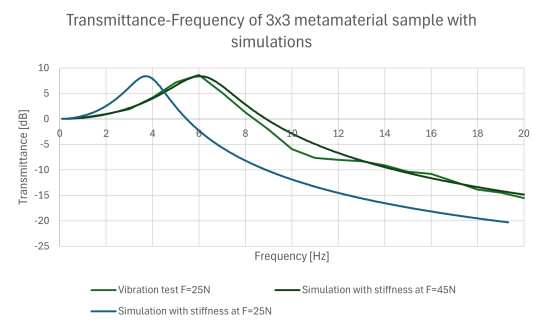

Figure 17: Transmittance-Frequency graph of 25N and simulations with a stiffness obtained from F=25N and F=45N

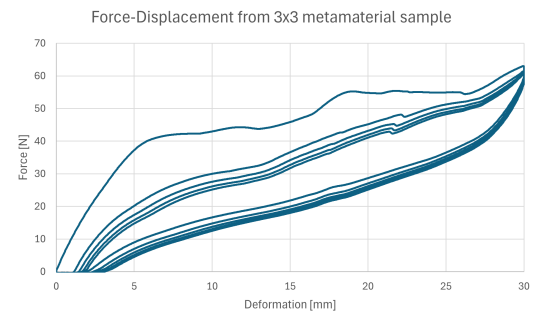

Figure 18: Force-Displacement of 3x3 metamaterial sample

An approach to verify the resulting transmittance-frequency graph is to compare the results of the physical test with a simple mass-spring system using the stiffness obtained from the 3x3 metamaterial compression test (Figure 18). The results from the vibration test using a loading force of 25N (20kPa) are presented in Figure 17.

For reference, this figure contains the results of two simulated mass-spring systems using the same mass, corresponding to a loading of 25N, but different values for stiffness. One stiffness is obtained from the static compression test around the loading force value of 25N. The other stiffness is obtained from the same static compression test around the loading force value of 45N. Both of these stiffness values are the result of taking the average stiffness of the loading branch and the unloading branch. Using the average stiffness results in a much more accurate simulation. When observing Figure 17, it can be seen that the simulation for 25N and the actual test for 25N do not overlap. However, the simulation for 45N overlaps with the actual test for 25N.

3.3 Force-induced static compression test

One of the results from the vibration tests indicated that the uncompressed shape reduces size after several compressions. To understand this phenomenon, a static compression test is performed with the force oscillating between two chosen values. The expected result of this test is to see a clear shift in displacement (or strain) during the force oscillations. The oscillating

force values are chosen around the relatively low stiffness region, which are obtained from the displacement-induced static compression test.

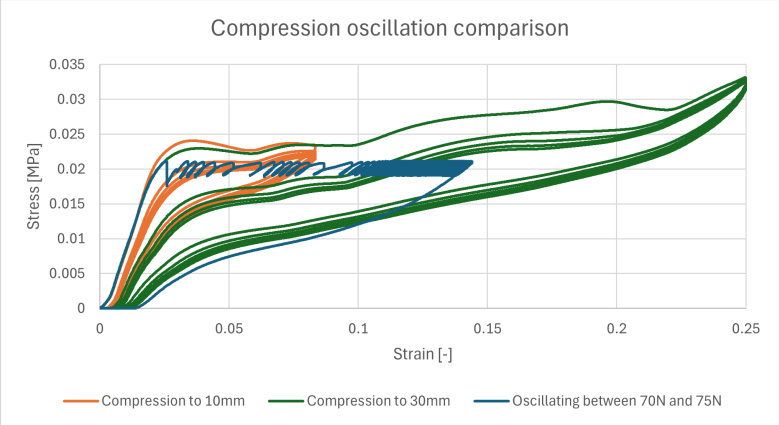

Figure 19: Quasi-static compression test results on a metamaterial sample

The results of the quasi-static compression tests using an oscillating force on one sample is presented in Figure 19. In this graph three curves are presented: one compression to 10mm, one compression to 30mm, and a compression with the force oscillating between 70N and 75N for 50 cycles. The oscillating force values are chosen based on the small QZS region for the 10mm compression test. Moreover, this test sample is a different 3x3 metamaterial test sample than used previously due to this sample being more stiff. This increased stiffness helps in visualizing the effect of the force oscillation. When observing the force oscillating curve, a clear displacement (or strain) shift can be seen. This shift proves that the uncompressed metamaterial sample continues to compress after several compressions. In addition, this displacement shift starts large and reduces after more oscillations. Moreover, the displacement shift stops roughly around the expected location between the loading branch and unloading branch. This confirms that in the simulations of the vibration tests must be performed using an average stiffness of the loading- and unloading branch.

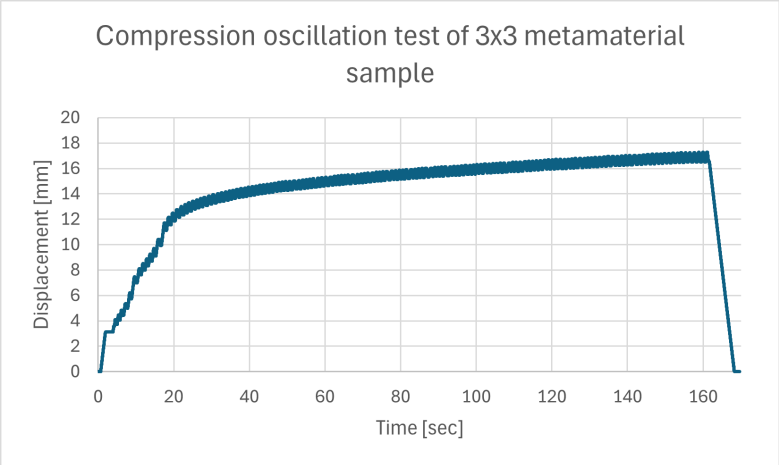

Figure 20: Oscillation test results of a 3x3 metamaterial

How large the reduction of displacement shift is can be seen from Figure 20, where the time is plotted against the displacement. In this graph, it can be seen that a large displacement shift occurs during the first 20 seconds, and after that a steady incline is shown.

4 Discussion

Within this chapter all results are interpreted, their meaning and significance are described, and it will be discussed how they relate to previous research. In addition, the limitations of this study are acknowledged, and implications for future work and broader context are suggested.

This chapter is separated into two sections. The first section discusses the results of the compression tests of both the single unit cell and the metamaterial sample, including a comparison between the boundary conditions. The second section discusses the dynamic vibration test results, including the comparison with a mass-spring system and a force oscillating compression test that confirms the observations discussed during the vibration tests.

4.1 Compression tests

This section of the discussion covers the information gathered during the initial compression tests. From the single unit cell overview (Figure 7), several behavior characteristics present themselves. The first characteristic is the stress peak during the first compression at low strain. This peak is caused by the initial buckling of several beams within the design. During consecutive compressions, this peak disappears. This disappearance is caused by the buckling beams having no pre-buckling phase, as the material is not perfectly reformed within the time frame of these compressions. Moreover, the stress-strain curve of these consecutive compressions do not remain constant but tend towards a limit cycle. This is caused by the viscosity of the material. The material does not have enough time between the compressions to reshape to the original shape, resulting in a shift towards a limit cycle. This limit cycle is separated in two sections, a loading branch and an unloading branch. There is a difference between these two branches due to the hysteresis effects, which can be attributed to by internal friction and visco-plastic effects. [30, 31]

In Figure 7, when comparing the 2D beam-node model results to the full 3D model, a stress difference in de QZS region can be observed. This difference could be caused by the 'thin beam' assumption in the 2D beam model, as the full 3D model is more accurate to the physical compression test. For the thin beam assumption, a thickness over length ration of 1/10 is the minimum for this assumption to be accurate, while this model has a thickness over length of 0.7/10.[32]

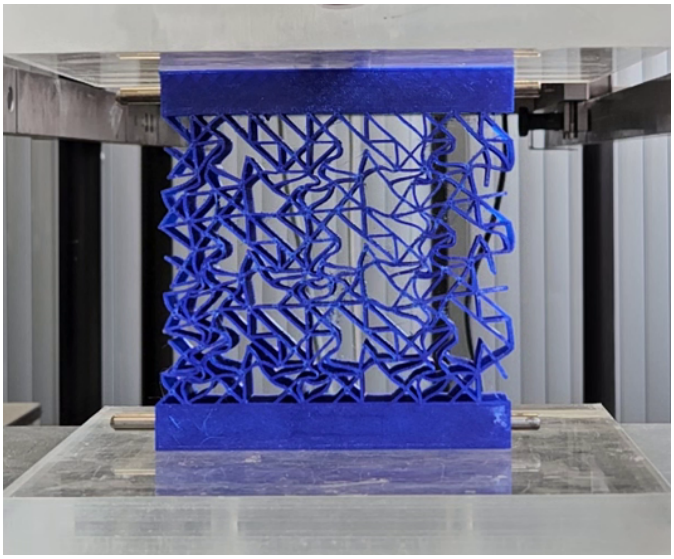

Figure 21: Visualisation of individual unit cell collapse

The 3x3 metamaterial compression test result does not exhibit the behavior that was expected. Instead of a QZS region, the sample behaves similar to a spring. However, there are two locations where a sudden stiffness change occurs. This specific change in stiffness can be explained by the collapse of individual unit cells, which is verified when physically inspecting the sample during the compression test. Figure 21 presents the compression of a metamaterial sample where the most deformations are visible at the bottom and the least at the top. This difference in deformation in each row indicates a separate collapse of each row. The difference between expectations and reality can be explained by the limited size of the metamaterial. With the 3x3 metamaterial sample each unit cell has unique boundary conditions, while the goal is to have the unit cells constrained identical as to identify it as a material instead of a structure. However, this is not feasible with the 2D beam model and the current manufacturing process as the 2D beam model assumes thin beams. To satisfy the assumption of thin beams, a larger structure is necessary, and thus, a maximum of three by three unit cells is possible.

Although the behavior of the 3x3 metamaterial is not what was expected, it can be interesting to identify which boundary conditions have a dominant effect on the stress-strain curve. Therefore, two additional metamaterial samples are tested, a 1x3 sample and a 3x1 sample. The first noticeable result shows that the stress-strain curves of all four (1x1, 1x3, 3x1, and 3x3) samples lie within a reasonable distance of each other. This proves that the conversion from force-displacement to stress-strain can be used to compare the different structure sizes. From the results it can be seen that the 1x1 single unit cell sample and the 1x3 metamaterial sample show a similar behavior. Therefore, it can be said that the row boundary conditions have a less dominant effect on the behavior of the structure. When comparing the 3x1 metamaterial sample to the 1x1 single unit cell sample, a larger difference can be observed. Therefore, it can be said that the column boundary conditions are very dominant in the behavior of the sample.

The size of the unit cell can have a significant influence on the performance of the optimized structure. A minimum size is required to obtain a cheap optimization process, however, enough variables must be availible to ensure the effectiveness of the optimal design. With a size of 3, the resulting optimal structure corresponds to an insufficient fitness. The size of 5 does result in an optimal structure with a sufficient fitness. In addition, the manufacturing process limits the thickness of the beams, resulting in a maximum size of 5 while complying with the 'thin beam' assumption. In theory, an optimal size should exist, higher and lower sizes should result in a less optimal structure. However, this theory is not further investigated during this project.

4.2 Dynamic vibration tests

This section of the discussion covers the information gathered related to a dynamic vibration tests and the respective simulations. Transmittance describes the difference in vibrations between two measurement points. The transmittance is calculated by obtaining the ratio in displacements of the top and bottom of the sample. This ratio is then converted to the frequency domain to obtain a frequency-transmittance plot. A positive transmittance indicates larger vibrations at the top of the sample compared to the bottom of the sample, zero decibel transmittance indicates equal vibrations at the top and bottom of the sample. Negative transmittance indicates smaller vibrations at the top of the sample compared to the bottom of the sample, which is the preferred behavior. A transmissibility of -10dB indicates that only about 30% of the input vibration amplitude is transmitted. Transmissibility approaching -20dB indicate even stronger vibration isolation.[33]

One detail from the transmittance-frequency curves that are provided in Figure 15 is that a resonance peak occurs. At the resonance peak, the input vibrations match the natural frequency of the system. Therefore, this peak represents the highest transmittance. The vibration isolation occurs at frequencies after the resonance peak. Therefore, a resonance peak at low frequencies is preferred. During the vibration tests, several loading conditions have been applied to the sample, resulting in different transmittance-frequency curves. In Figure 16, it can be observed that there is a range of loading conditions that perform better related to this resonance frequency. When relating this to the stress-strain curves obtained during the compression tests, a prediction is done that for specific stress levels, a lower stiffness is obtained. This ideal range of loading conditions suggests that there is a loading force that corresponds to the prediction made. In addition, when focussing on the three loading conditions with the lowest resonance frequency (20N, 25N, and 30N), it can be seen that both the 20N and the 30N resonance peaks have broad peaks compared to the 25N narrow peak. This difference in peak indicates the uncertainty of the resonance frequency. Every 1Hz a measurement is taken, therefore, it is very possible that 25N would have resonance peak slightly less than 6Hz while the 20N and 30N would have a resonance peak at a frequency slightly higher than 6Hz. Therefore, it can be said that the 25N loading condition with the narrow peak indicates the optimal loading condition for this specific sample.

The vibration isolation test can be compared to a simple mass-spring system if the test sample is considered the spring. The stiffness of the test sample (or spring) can be obtained through the static compression stress-strain curve. Specifically, the stiffness corresponds to the average of the slope of the loading branch and the unloading branch at a force is 25N. For example, the simulation corresponding to the test with a loading condition of 25N consist of a mass of 25N and a spring with a stiffness of 1.5N/mm. In this example, the spring is assumed to be massless as the weight of the spring is negligible compared to the 25N loading. From Figure 17, it can be observed that the simulation of the 25N setup does not correspond to the simulation of the 25N setup. However, a simulation using the same mass but a stiffness from around the 45N range seems to correspond to the 25N test results. The question arises why the test sample under loading conditions of 25N responds with a stiffness that corresponds to a sample loaded by 45N. When visually inspecting the sample during the test, it can be observed that the size of the sample changes over time (for the sample frequency and loading), see Figure 22 with the size indicated by the ruler on the left side. To translate this to the stress-strain curve, a displacement (strain) shift occurs over time. This indicates a shift in stiffness, which explains the large difference that is observed from the simulation comparison.

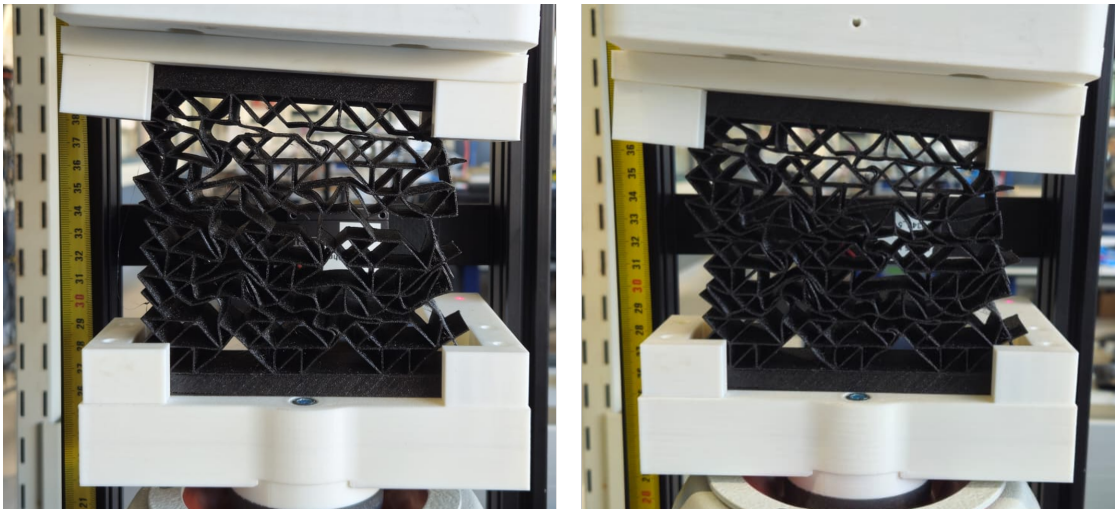

Figure 22: Visualisation of before (left) and after (right) vibration testing

To confirm the theory that the size of the structure reduces when consecutive compressions occur, compression oscillation tests are preformed, see Figure 19. The displacement shift is visualized in the stress-strain curve by a shift in the positive strain direction during the force oscillations. The reason for this displacement shift can be explained by a couple of causes. The first cause is the viscosity of the material. The material does not have enough time to reshape in its original configuration, therefore, each oscillation a small strain occurs.[31]

From the oscillation compression test result it can be seen that the speed of the displacement shift is not constant. This is also visible from Figure 20, which presents the displacement-time graph. From this graph can be concluded that there is a large displacement shift during the first several oscillations, which slows down after more time passes. The speculated end location, where the displacement shift is done, is between the loading and unloading branch. This verifies why a stiffness needs to be obtained from the average slope of the loading and unloading branch.

What is observed is that the design for the metamaterial sample is not optimal for vibration isolation purpose. The main cause of the unpredicted behavior is the stiffness shift that occurs during repeated compressions, which are not included in the optimization process and the static model. A large reason for this stiffness shift is related to the material and the boundary conditions. Therefore, using a material with less viscosity prevents most of the stiffness shift.[31] In addition, increasing the size of the metamaterial, which is for this research no more than three by three, will provide a more accurate representation of the model and final goal.

5 Conclusion

This study set out to identify the vibration isolation behavior of an optimized simple beam-node structure. This goal is achieved by answering the following main question: "To what extent does a simplified 2D simulation model of a beam-node metamaterial designed for quasi-zero stiffness accurately predict its experimentally observed static and dynamic behaviors?". To answer this question, firstly, a simple structure consisting of horizontal, vertical, and diagonal beams was optimized using a genetic algorithm optimization process. Then, the optimized structure was produced using FDM 3D printing with TPU material. These produced samples have been tested using a static compression test and a dynamic vibration test. These test results and the simulations were compared to identify the accuracy of the 2D beam-node model.

During the compression tests, several notable behavior properties are presented. The first notable behavior of all the samples is the difference between the first compression and the last compression. Specifically, the tendency to behave as a limit cycle during consecutive compressions. This behavior is the effect of viscosity in the material. Moreover, this viscosity partially explains the initial peak for the single unit cell compression tests, as this peak disappears after several consecutive compressions. In addition, the difference between the loading and unloading branches can be explained by the hysteresis effects due to internal friction and visco-plastic effects. However, the metamaterial samples do not behave as predicted, as there is no QZS region. One of the most obvious explanations is the limited size of the metamaterial. Having only three by three unit cells is not enough to reduce the boundary effects of the total structure. However, the influence of row constraints compared to column constraints are significant. Moreover, the row constrained (1x3 metamaterial) has similar behavior to the single unit cell sample. The column constrained (3x1 metamaterial) has similar behavior to the full 3x3 metamaterial. Therefore, the column constraints have a dominant effect on the behavior of the full metamaterial sample. Since the samples are loaded vertically, more forces are applied through the column constraints, and thus these constraints are more critical.

During the dynamic vibration testing, several different loads are applied. The results of these tests indicate the presence of an optimal loading condition for vibration isolation. Specifically, in the resonance frequency-loading force graph (Figure 16) a minimum resonance frequency exists between 20N and 30N. Furthermore, the optimal loading condition is 25N, which is indicated by the shape of the transmittance-frequency curve. This curve presents a narrow peak compared to 20N and 30N which have a shallow peak.

When comparing the transmittance-frequency graph of the 25N test sample to a simple mass-spring system using equal mass and the spring stiffness obtained from the static compression force-displacement curve, a large difference is identified. More specifically, the test results of the 25N sample are effectively identical to a simple mass-spring system using equal mass but with the spring stiffness obtained from the static compression force-displacement curve at a loading condition of 45N. This indicates a displacement shift during the vibration tests, which are visually verified.

Further verification of this displacement shift is obtained with a force-oscillating compression test. The results of this test indicate a displacement shift with an initial high displacement, which slows down stopping between the loading and unloading branch. The displacement shift is possibly caused by the viscosity in the material, as there is not enough time for the structure to fully reform back to its original shape.

The findings show that a simplified 2D beam-node model can reasonably well predict the static QZS behavior for single unit cells. However, for metamaterials consisting of a small number of unit cells, the 2D beam-node model deviates severely from the observed experiments. This deviation is partially caused by the limited number of unit cells and by the displacement shift during the vibration tests.

The purpose of this thesis is to identify the static and dynamic behavior of an optimized design. The optimization process has been used to obtain several testing samples. However, the optimization process is to obtain a desing with a QZS region that can be tested. The objective is to obtain a working desing, not the most optimal design. In addition, only one material (TPU) has been used during the testing phase.

This study combines the knowledge of metamaterials, optimization of 2D beam-node models, and vibration isolation. As a result, this research highlights the possibility of obtaining simple metamaterial design for the purpose of vibration isolation through a relatively fast optimization process.

For future research, it is recommended to further test larger metamaterial samples, for example ten by ten unit cells. However, it should be mentioned that the 2D beam-node model assumes thin beams. Therefore, if the length of the beams is decreased, the thickness should decrease accordingly. Another research topic that could be significant is experimenting with different materials to attempt a reduction of the displacement shift.

Ultimately, this thesis project combined three unrelated subjects to provide a foundation for a new potential approach to vibration isolation metamaterial. The results show that a simplified beam-node model captures the key static behavior of a single unit cell, while deviations occur for small metamaterials. Even though the dynamic vibration results are not what was expected according to the model, the source of this dynamic behavior is identified and explained through additional testing. The combination of knowledge on the relation between the beam-node models and the static and dynamic tests on the vibration isolation metamaterial provides a foundation for future research.

References

[1] Xuan Li et al. "Design and characterization of a compact tripod quasi-zero-stiffness device for isolating low-frequency vibrations". In: *Precision Engineering* 91 (Dec. 2024), pp. 632–643. ISSN: 01416359. DOI: 10.1016/j.precisioneng.2024.10.013.

[2] Feng Liu et al. "Total reflection of flexural waves by circular meta-slab and its application in vibration isolation". In: *International Journal of Mechanical Sciences* 212 (Dec. 2021). ISSN: 00207403. DOI: 10.1016/j.ijmecsci.2021.106806.

[3] Shuai Guo, Shutian Liu, and Renjing Gao. "A bidirectional quasi-zero stiffness metamaterial for impact attenuation". In: *International Journal of Mechanical Sciences* 268 (Apr. 2024). ISSN: 00207403. DOI: 10.1016/j.ijmecsci.2024.108998.

[4] Xiuting Sun and Xingjian Jing. "A nonlinear vibration isolator achieving high-static-low-dynamic stiffness and tunable anti-resonance frequency band". In: *Mechanical Systems and Signal Processing* 80 (Dec. 2016), pp. 166–188. ISSN: 10961216. DOI: 10.1016/j.ymssp.2016.04.011.

[5] C. Drezet, N. Kacem, and N. Bouhaddi. "Design of a nonlinear energy harvester based on high static low dynamic stiffness for low frequency random vibrations". In: *Sensors and Actuators, A: Physical* 283 (Nov. 2018), pp. 54–64. ISSN: 09244247. DOI: 10.1016/j.sna.2018.09.046.

[6] Yawei Zheng et al. "Design and modeling of a quasi-zero stiffness isolator for different loads". In: *Mechanical Systems and Signal Processing* 188 (Apr. 2023). ISSN: 10961216. DOI: 10.1016/j.ymssp.2022.110017.

[7] Alexandra Ion et al. "Metamaterial mechanisms". In: *UIST 2016 - Proceedings of the 29th Annual Symposium on User Interface Software and Technology*. Association for Computing Machinery, Inc, Oct. 2016, pp. 529–539. ISBN: 9781450345316. DOI: 10.1145/2984511.2984540.

[8] David Restrepo, Nilesh D. Mankame, and Pablo D. Zavattieri. "Programmable materials based on periodic cellular solids. Part I: Experiments". In: *International Journal of Solids and Structures* 100-101 (Dec. 2016), pp. 485–504. ISSN: 00207683. DOI: 10.1016/j.ijsolstr.2016.09.021.

[9] Pengcheng Jiao et al. "Mechanical metamaterials and beyond". In: *Nature Communications* 14.1 (Dec. 2023). ISSN: 20411723. DOI: 10.1038/s41467-023-41679-8.

[10] Ramin Hamzehei, Mahdi Bodaghi, and Nan Wu. *Mastering the art of designing mechanical metamaterials with quasi-zero stiffness for passive vibration isolation: a review*. Aug. 2024. DOI: 10.1088/1361-665X/ad5bcc.

[11] Bingxiao Ding et al. "Modular quasi-zero-stiffness isolator based on compliant constant-force mechanisms for low-frequency vibration isolation". In: *JVC/Journal of Vibration and Control* 30.13-14 (July 2024), pp. 3006–3020. ISSN: 17412986. DOI: 10.1177/10775463231188160.

[12] Haigui Fan et al. "Design of metastructures with quasi-zero dynamic stiffness for vibration isolation". In: *Composite Structures* 243 (July 2020). ISSN: 02638223. DOI: 10.1016/j.compstruct.2020.112244.

[13] Ji Liu et al. "Customized quasi-zero-stiffness metamaterials for ultra-low frequency broadband vibration isolation". In: *International Journal of Mechanical Sciences* 269 (May 2024). ISSN: 00207403. DOI: 10.1016/j.ijmecsci.2024.108958.

[14] Shuai Guo et al. “A quasi-zero-stiffness elastic metamaterial for energy absorption and shock attenuation”. In: *Engineering Structures* 280 (Apr. 2023). ISSN: 18737323. DOI: 10.1016/j.engstruct.2023.115687.

[15] Kuan Liang, Yuhui Jing, and Xiaopeng Zhang. “Design of broad quasi-zero stiffness platform metamaterials for vibration isolation”. In: *International Journal of Mechanical Sciences* 281 (Nov. 2024). ISSN: 00207403. DOI: 10.1016/j.ijmecsci.2024.109691.

[16] V S Deshpande, M F Ashby, and N A Fleck. *Foam topology bending versus stretching dominated architectures*. Tech. rep. 2001, pp. 1035–1040. URL: www.elsevier.com/locate/actamat.

[17] Jinyong Joo, Sridhar Kota, and Noboru Kikuchi. “Topological synthesis of compliant mechanisms using linear beam elements”. In: *Mechanics of Structures and Machines* 28.4 (Nov. 2000), pp. 245–280. ISSN: 08905452. DOI: 10.1081/SME-100102022.

[18] Chiara Bregoli et al. “Mechanical response of LPBFed TI64 thickness graded Voronoi lattice structures”. In: *Materialia* 38 (Dec. 2024). ISSN: 25891529. DOI: 10.1016/j.mtla.2024.102234.

[19] J. Martínez et al. “Star-shaped metrics for mechanical metamaterial design”. In: *ACM Transactions on Graphics* 38.4 (2019). DOI: 10.1145/3306346.3322989.

[20] inc. The MathWorks. *MATLAB*. Natick, MA, USA, 2025.

[21] COMSOL AB. *COMSOL Multiphysics*. Stockholm, Sweden, 2025.

[22] COMSOL AB. *COMSOL Multiphysics Reference Manual Version 6.4*. Tech. rep. Stockholm, Sweden: COMSOL AB, 2025. URL: https://doc.comsol.com/6.4/docserver/#!/com.comsol.help.comsol/helpdesk/helpdesk.html.

[23] A. Saxena. “Topology design of large displacement compliant mechanisms with multiple materials and multiple output ports”. In: *Structural and Multidisciplinary Optimization* 30.6 (Dec. 2005), pp. 477–490. ISSN: 1615147X. DOI: 10.1007/s00158-005-0535-z.

[24] Changqi Cai et al. “Design and numerical validation of quasi-zero-stiffness metamaterials for very low-frequency band gaps”. In: *Composite Structures* 236 (Mar. 2020). ISSN: 02638223. DOI: 10.1016/j.compstruct.2020.111862.

[25] Zachary Satterfield et al. “Unit cell synthesis for design of materials with targeted nonlinear deformation response”. In: *Journal of Mechanical Design* 139.12 (Dec. 2017). ISSN: 10500472. DOI: 10.1115/1.4037894.

[26] Mathworks. *Mathworks Documentation GA function*. 2025. URL: https://nl.mathworks.com/help/gads/ga.html.

[27] ColorFabb. *colorFabb TPU85A*. Tech. rep. 2024. URL: https://downloads.colorfabb.com/index.php/s/rtfDDRCa723Xdor?dir=/Technical%20Data%20Sheets/TPU/colorFabb%20TPU85A&editing=false&openfile=true.

[28] Zwick Roell. *Product Information Materials Testing Machines ProLine Z005 to Z100*. Tech. rep. 2025. URL: https://www.zwickroell.com/fileadmin/content/Files/SharePoint/user_upload/PI_EN/02_375_ProLine_Z005_up_to_Z100_Materials_Testing_Machine_PI_EN.pdf.

[29] Schwingtechnik Vibration Test Systems. “Tira Vibration Test System TV 51110”. In: (2014).

[30] M. Bodaghi et al. “Reversible energy absorbing meta-sandwiches by FDM 4D printing”. In: *International Journal of Mechanical Sciences* 173 (May 2020). ISSN: 00207403. DOI: 10.1016/j.ijmecsci.2020.105451.

[31] Roderic S Lakes. *VISCOELASTIC*. Tech. rep. 1998. DOI: https://doi-org.tudelft.idm.oclc.org/10.1201/9781315121369.

[32] R. C. Hibbeler. *Mechanics of Materials Tenth Edition in SI Units*. Tech. rep. 2018. URL: www.pearsonglobaleditions.com/hibbeler.

[33] Cyril M.. Harris and Allan G.. Piersol. *Harris' shock and vibration handbook*. McGraw-Hill, 2002. ISBN: 0071370811.

DELFT UNIVERSITY OF TECHNOLOGY

LITERATURE REVIEW

Optimization Methods for Network-Based Metamaterial

Literature review

Author:
Duran Manshanden (5647347)
January 21, 2026

***Abstract*—Mechanical vibrations often occur in moving structures such as robotic arms or 3D printers. When these machines experience high external vibrations, their overall performance is reduced. To mitigate this, a vibration isolation metamaterial could be used. This review provides an overview of three aspects of the design for optimal vibration isolation metamaterial. The first aspect covers how vibration isolation can be obtained using the quasi-zero stiffness method (QZS) and what design approaches are typically used. The second aspect covers the beam-node model that is used and the benefits this could have. The third aspect covers the optimization process, with special attention to various optimization methods compared to predefined characteristics.**

I. Introduction

Mechanical vibrations often occur in moving mechanical structures such as robotic arms or 3D printers. The overall performance of these machines is reduced when high external vibrations are present. Therefore, various linear vibration isolation structures have been designed to minimize this deteriorating effect. These structures isolate specific frequency bands and generally have a large and complex shape. An alternative to such large isolation structures is the use of emerging properties in special designed metamaterial. The benefits from using metamaterial is to reduce failure points, complexity, and overall moving parts while enhancing performance.

Several attempts have been made to design such a vibration isolation metamaterial.[1]–[8] Not many of these designs are optimized and those that are have a very limited optimization process, for example a design where only the size is optimized and not the shape. Size optimization is very dependent on the initial design, potentially resulting in a sub-optimal solution. Optimizing the shape of these designs require a lot of computational power, especially when a full finite element method (FEM) model will be used. Therefore, this literature review is focused on a model constructed from a set of beams connected by ball-joints (nodes). Further focus of this literature review is placed on how vibration isolation is achieved using quasi-zero stiffness (QZS) and how to approach such a design. The final focus of this review is on different optimization methods that can be applied to a QZS problem. The goal of this literature review is to present an overview of different methods and approaches to design and optimize a vibration isolation metamaterial.

This literature review is constructed as follows. The methods for collecting relevant literature and categorizing them is presented in section II. A general overview of how to design for QZS with corresponding examples and validation methods is presented in section III. A detailed explanation on the beam-node model and how this can be modelled efficiently as a metamaterial is presented in section IV. All the relevant optimization methods are presented in section V. Both the QZS design approach, the model, and the optimization methods are discussed in section VI, followed by a conclusion in section VII.

II. Research methodology

During the process of writing the literature review many sources are discussed. The goal of this review is to present what has been done and what is yet to be done. Therefore, it is essential to ensure all relevant papers are covered. A research methodology provides a systematic approach to ensure all relevant papers are covered.

For this literature review, the Scopus database is used to find relevant papers using the terminology provided in Table I. The search includes all papers published before January 1, 2025. Different spellings of specific terms and synonyms are implemented to ensure full coverage of papers.

The research is done in three phases. First, research is done for QZS and metamaterial, using the first and second column of Table I. For the second (the model) and third (optimization) phase a combination of the first, third, and fourth columns are used with varying amount of columns. With varying amount of columns is meant that when too few papers where obtained fewer columns are used, and when too many papers where obtained more columns are used.

Table I: Overview of search terms

	AND			
	Metamaterial	QZS	Optimization	Beam-node
	Meta-material	Vibration isolation	Topology optimization	Truss
OR	Micro lattices		Shape optimization	Members & hinges
	Lattice material		Size optimization	Ball-pivot
			Genetic algorithm	

III. The design of QZS mechanisms

In this section the approach on how QZS mechanisms are designed is discussed, including how these designs are validated for their QZS properties. First, a brief introduction on what QZS is and what the two methods are to obtain a QZS design are described (Positive & negative stiffness elements, buckling). Second, both methods will be further described, supported by examples. Finally, common validation methods are provided which are used in all research.

The QZS region of a mechanism is a range where motion occurs without requiring additional energy. This allows the mechanism to isolate certain vibrations within the QZS region. However, very low-frequency vibrations are not always isolated because the effective stiffness is not always zero but near zero. Figure 1 shows a typical force-displacement curve for a design with a QZS region. For small displacements the force increases (positive slope), meaning this design has a positive effective stiffness for that specific range of motion. After a certain displacement threshold, the force stabilizes and a plateau appears where a certain range of motion is applicable around a specific force, meaning the effective stiffness is zero. This range of motion is also called the QZS region. After a second displacement threshold, the force increases again and the design regains a positive effective stiffness.

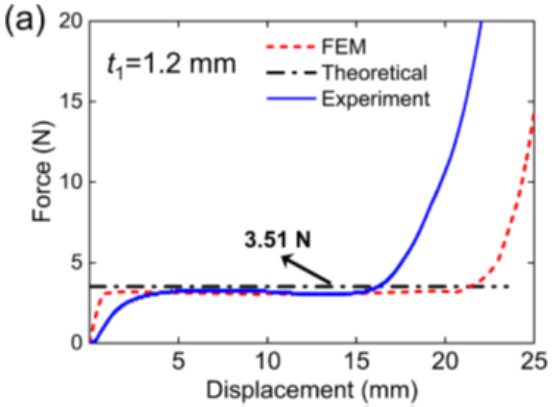

Figure 1: Typical force-displacement curve of a QZS design.[6]

There are two common methods for designing a structure with a QZS region. The most common method combines positive and negative stiffness elements in a structure. When these opposing stiffness elements overlap, they create a QZS region. Often the negative stiffness element is obtained using bi-stability. A less common approach uses the nonlinear properties of buckling. As a structure buckles, its displacement becomes highly nonlinear, exhibiting a softening behavior, the structure becomes more flexible, allowing larger deformation for a given force change.[9]

A. Example of QZS design

Positive and negative stiffness elements

One method to achieve quasi-zero-stiffness in a system is by combining two sections: a negative stiffness (NS) and a positive stiffness (PS) section. These sections counteract each other to create a near-zero stiffness region.[9]

The positive stiffness elements exhibit a linear relationship between applied force and displacement as they resist deformation. In contrast, the negative stiffness element shows opposite behavior, applied force and displacement have inverse signs.[9] When these elements are combined in a specific configuration, they create a QZS region. At small deformations, the positive stiffness element dominates. As the deformation (or applied force) increases, the negative stiffness element activates, reducing the mechanism's overall effective stiffness. Beyond a certain threshold, the positive stiffness element regains dominance. This process is presented in Figure 2. The first part labelled DSM represents the PS element with a positive linear force-displacement relation. The second part labelled BSB represents the NS element. The non-linear negative stiffness of this element is obtained through bi-stability. The third part labelled CCFM is the combined structure, where the working range represents the QZS region.

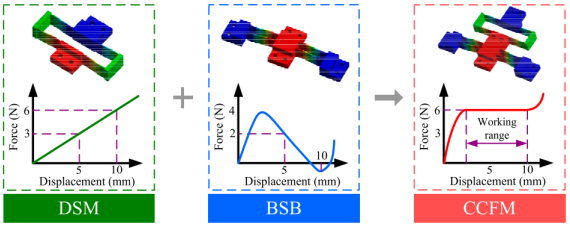

Figure 2: Schematic of forcedisplacement curves of positive and negative-stiffness components superposition for zero stiffness. [10]

A classic example of such a system is the one described by Fan et al [1]. In this paper a unit cell consists of a sinusoidal beam, several semicircular arches, and stiffer walls. The sinusoidal beam demonstrates negative stiffness properties under lateral load, while the bending-dominant arch exhibits positive stiffness properties under vertical load. When these two elements are arranged appropriately, a QZS property emerges. The design's QZS region can be optimized by adjusting the thicknesses and radii of the components.[1]

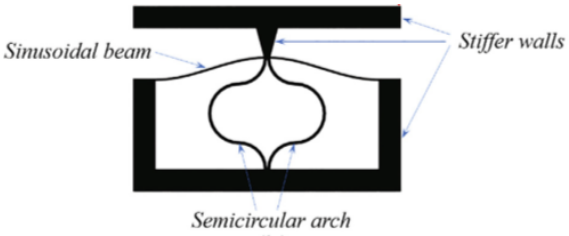

Figure 3: Unit cell formed by a sinusoidal beam and two semicircular arches. [1]

A very similar design is described by Liu et al in 2024 [2], where a heart-shaped structure (PS) and a cosine beam (NS) are used to obtain a QZS region, see Figure 4(a). Another design of a bidirectional QZS metamaterial is described by Guo et al in 2024 [3], [4], presented in Figure 4(b). In this paper two parallel cross-curved beams, which represent negative stiffness, and a ring parallel to the cross-curved beams, representing positive stiffness, are combined. Additionally, Zheng [5] describes a design that combines a pair of identical oblique beams (NS), three stiffer walls, and a pair of identical semicircular arches (PS), with the negative and positive stiffness elements arranged in parallel, see Figure 4(c). The final notable design is described by Liang [6], presented in Figure 4(d). He describes a design consisting of only horizontal and diagonal beam elements. Here the NS property is caused by unstable buckling of the diagonal beams and the PS property is caused by the contact of the deformed diagonal beams and the horizontal beams.

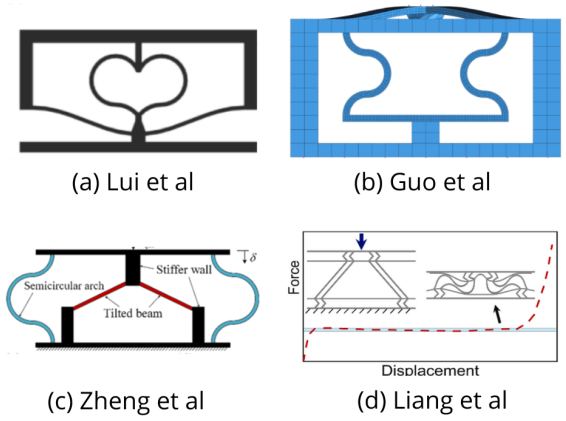

Figure 4: (a) Representation of the heart-shaped structure unit cell in initial state and in compression state [2] (b) Bidirectional QZS unit cell consisting of two parallel cross-curved beams and a positive stiffness ring [4] (c) Unit cell consisting of a pair of identical oblique beams and a pair of identical semicircular arches [5] (d) Design based on horizontal and vertical beams only [6]

Buckling design

An alternative method to achieve QZS in a system is by using the nonlinear properties of buckling. A paper by Zhang in 2021 [7] describes a QZS structure based on buckling. The proposed vibration isolation metamaterial consists of a unit cell with a simple load-carrying block supported by two curved beams. Each beam is designed with six control points, carefully selected to achieve a QZS zone. A genetic algorithm generates a spline that runs through these points. Unlike previous examples, this design achieves its QZS properties solely through beam buckling. [7]

Due to the configuration of this design, the compression force acting on the structure solely goes through the two curved beams. Therefore, the maximum force for this design approach is much less than the other two design approaches, as those are supported by positive stiffness elements. The only method of increasing the zero-stiffness force in this design is to use a stronger material. Therefore, this approach is only applicable for lower zero-stiffness forces.

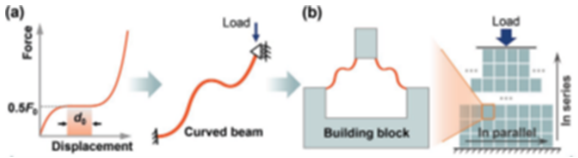

Figure 5: Schematic diagram of the design of mechanical metamaterials with programmable QZS features. [7]

Alternative optimization approach

Another interesting approach to obtaining QZS was developed by Xu Y in 2024.[8] In this study, a unit cell of predetermined size was optimized to minimize the difference between the metastructure's static response and the targeted force-displacement curve in the QZS region.[8] The targeted force-displacement curve shown in Figure 6(a) indicates the QZS zone as region II.

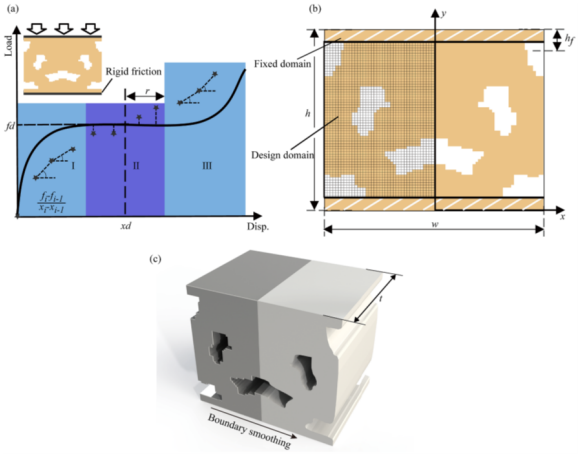

Figure 6: Mathematical model of topology optimization and schematic diagram of the design domain for a QZS metastructure. [8]

The model is created by starting with a grid of Nh by Nw pixels, see Figure 6(b). Each pixel has a value 1 (solid) or 0 (empty) assigned to it. As a starting point of the optimization algorithm the grid will be randomly perforated. During the genetic algorithm optimization process the value of each pixel will be changed until the optimized result is obtained in the force-deflection curve. This approach does not use any of the prescribed approaches for achieving the QZS property. However, in the simulations and in the tests, the nonlinear properties of buckling can be recognized.

B. Validation of QZS

There are two main methods to validate if the simulations of the design are made with the proper assumptions. The first method is to perform a simple compression test and compare the force-displacement curve of the experiment to the curve from the simulations. [6]–[8] Some examples of results are presented in Figure 7, 8 and 9.

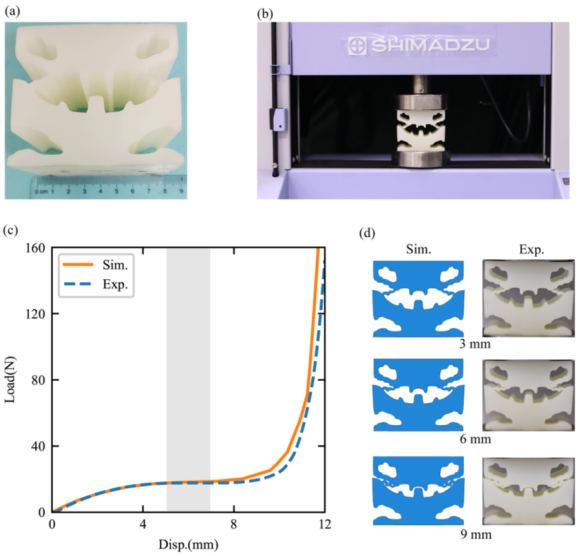

Figure 7: Experiments of the QZS metastructure. [8]

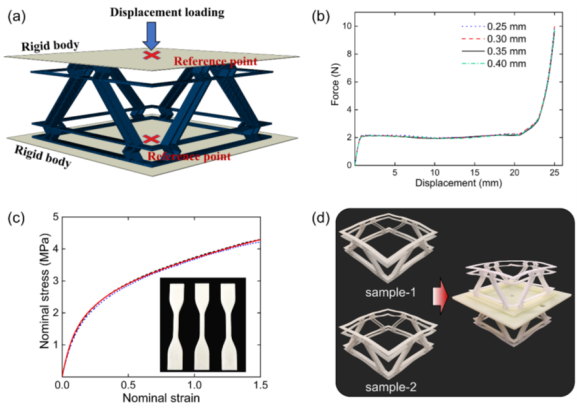

Figure 8: Finite element model of the designed unit cell and experimental samples fabricated using 3D printing technology. [6]

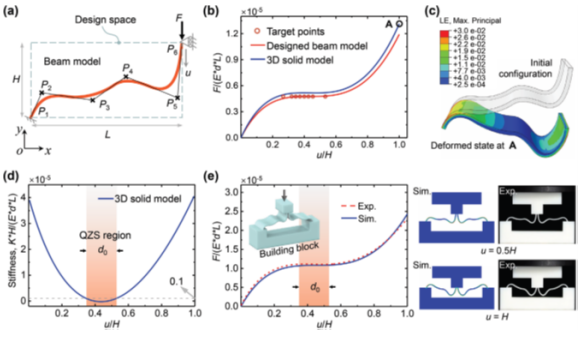

Figure 9: Mechanical behavior of the tailored curved beam, and the corresponding basic building block. [7]

The second method is to perform a vibration test with a shaker. For this method, several experiments with a shaker must be performed using different support masses to observe the region before the QZS region, the QZS region itself and the region after the QZS region. From the experiments, a transmittance-frequency graph is produced. To confirm the QZS region the transmittance becomes negative for the applied frequencies. This is clearly presented in Figure 10 and Figure 11.

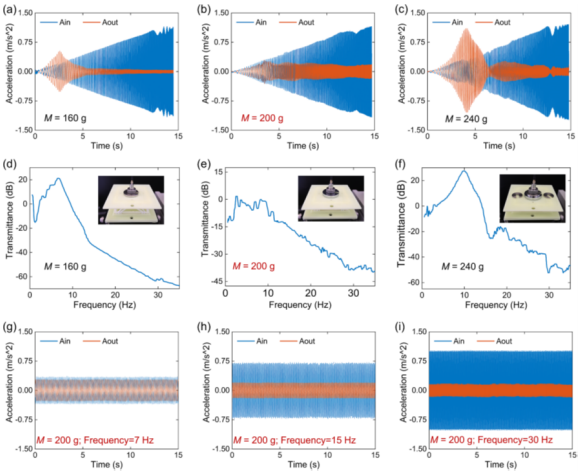

Figure 10: Vibration test results at different support masses. [6]

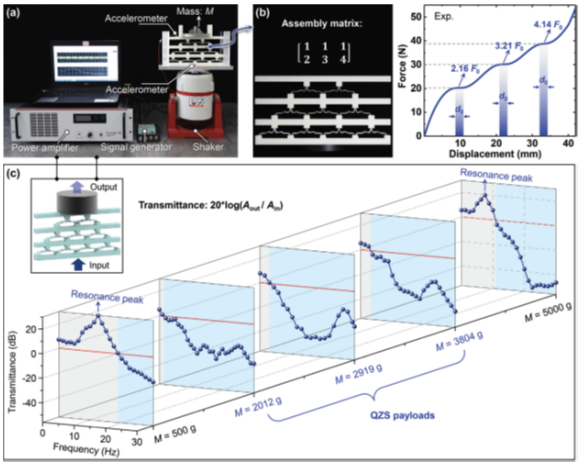

Figure 11: Experimental vibration tests. [7]

To reduce errors in the simulations, most design papers use a tensile test on dogbone specimens to obtain material properties that are used in the simulations. [6]
The results of compression tests are interesting for this subject. However, in most cases, only the curve for loading the structure is included in the literature. It can be interesting to observe the resulting unloading behavior of a unit cell, as there will be an unavoidable hysteresis effect that can have a significant influence on very low-frequency vibrations.

IV. Model

The focus of this literature review is on the optimization of QZS metamaterials. In the previous section, the QZS subject is covered. The next step is understanding how to model the QZS metamaterial. In this section, a beam-node network model approach will be explained with its respective benefits and drawbacks. The beam-node model is selected due to its computational efficiency and lower cost compared to traditional FEM models in optimization processes. Several example projects are discussed where the beam-node principle is used, each example provides a unique aspect, which could be used in future works.

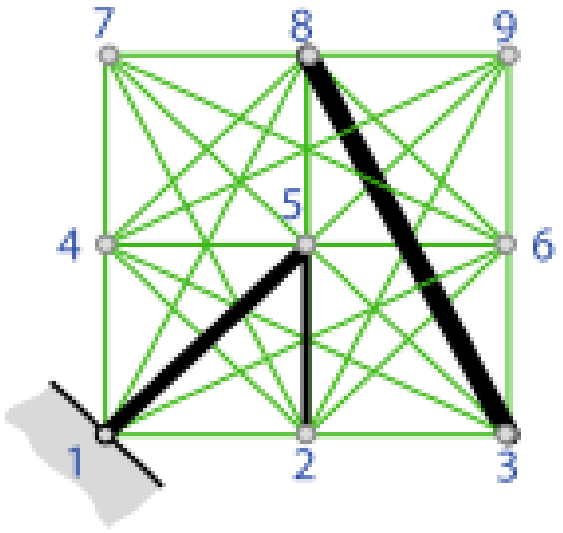

Figure 12: Example of the spanning tree method. [14]

A. *beam-node Network Model*

In general, structural optimization for synthesis of microstructures requires significant computational resources due to the high number of design variables[11], [12]. Therefore, in this literature review, a set of beams connected by ball-joints (nodes) are implemented as model. In this specific model the emphasis is placed on having few elements to reduce calculation costs. As a result, the model includes relatively long beam elements where the bending of the beams must be included in the calculations.

The most notable variables within a beam-node network model are the length of the beams, the cross-sectional area of the beams, and the material property of the beams.[13] Although these are the most notable variables, more variables can be added to obtain better optimized solutions. An example of such a variable could be a non-constant cross-sectional area.[13]

Danzi et al [14] wrote a paper describing a novel element removal method for ground structured base topology optimization. This process consists of two phases; Threshold limit removal (removing members whose cross-sectional area is under a lower bound), and graph based element search and cut (removing elements that are not reachable from specified root node).[14] The goal of the element removal method is to ensure the optimal solution can be physically realized. As the predecessor of this method, the ground structure method, often leads to complex designs that can be difficult to realize physically due to floating or non-connecting beams.[14] The ground structure method is based on the spanning tree theory, where spanning trees connect all the vertices together using a minimum number of edges within a predefined space.[15]

The main benefit of using the beam-node network model is to reduce calculational costs during the optimization part. Simulating non-linear calculations instead of multiple linear calculations results in a massive calculation cost reduction, which can lead to a reduction of tenfold.[16] Another benefit of the beam-node network model is that the number of variables during the optimization process can easily be adjusted. As an example the material properties can be fixed or can be variable, and the beams can be restricted to be vertical, horizontal, and diagonal only. Therefore, the model can be simplified or can be made more complex. This can be very useful to reduce additional costs when simplifying the model. For example as a preliminary design the material of all beams is assumed fixed, and only horizontal, vertical, and diagonal beams are used. Once this design is satisfactory, the angle of the beams can be added as a variable to make the design more complex and acquire more accurate results. Additionally, the cross-section area can be added as a design variable as well to enhance the complexity of the system.[17]

Although the beam-node network model can be seen as a very good alternative to other methods, it does have several drawbacks. One of these drawbacks is that the resulting design cannot always be manufactured. Therefore, there must be an additional smoothing step in the process.[17]

Research on periodic truss structures is done by Deshpande et al. [18]. In this study, Maxwell's criterion is used to define a condition for the deformation of periodic truss structure to be stretch-dominated. Interestingly, stretch-dominated truss structures are stronger than bending-dominated structures [11]. The stretching-dominated materials have a softening post-yield response

due to the buckling of struts.

In a paper written by J. Prasad a variation of the beam-node network model is used.[19] The structure in the paper is analyzed using nonlinear, corotational Timoshenko beam element and a total Lagrangian formulation.[20] The model consists of beam elements joint rigidity, which may be overestimated compared to a full 2D elasticity model. To overcome this drawback the cross-sectional area near the flexible joints will be reduced. An alternative to this solution is to model a soft rubber-like material near the hinges. [19] Therefore, in the present model, the beam members are divided into three regions as presented in Figure 13. The verification process in this paper is done by comparing the results of the beam element model with an ABAQUS model, using element "b21".

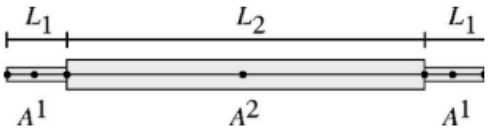

Figure 13: Example of a three way beam element. [19]

The paper written by Sauter [13] describes a design procedure using evolutionary optimization with a complex beam-node model. Within this model, beam elements with a complex shape, such as variable thickness (Figure 14) and curved centerline shape (Figure 15), are used. Castigliano's theorem is used for connecting the set of beam parameters with the beam's structural properties, as this is a good compromise between accuracy and numerical costs.[13] The parameters to describe one complex beam element are the four end-point coordinates, two centerline run-out angles (at end point), one length factor L, and four thicknesses at four points along the centerline.

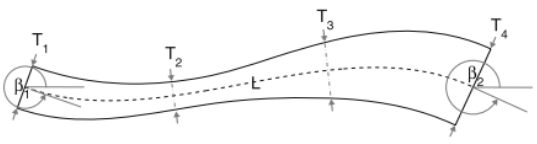

Figure 14: Curved beam with variable thickness. [13]

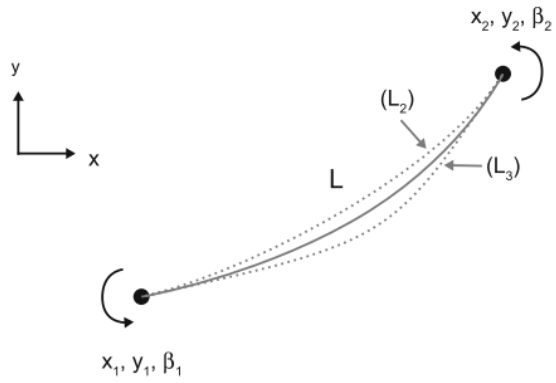

Figure 15: Curved beam with centerline defined by start- and endpoint parameters and factor L. [13]

A paper written by Jang [21] describes a design method for compliant mechanism consisting of standardized elements such as semi-rigid beams, hubs, and joints. The optimization problem is set up using standard ground-beam based topology optimization. The joints are modelled as short Timoshenko beam elements, see Figure 16. This is very compatible with the approach of Prasad [19], the same short beam elements with customized beam properties are used to represent joints.

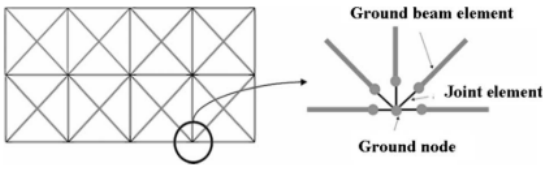

Figure 16: Proposed ground structure consisting of ground beam and joint elements. [21]

Many papers, that use a similar model, validate their findings by comparing it with a full FEM model.[16], [19] However, comparing the beam-node network model to a FEM model does require an additional smoothing step.[13] Other papers validate the design by comparing their findings with already existing designs that are tested.[13]

V. Optimization methods

In this section, the whole optimization process will be discussed. The first part provides insight into the objective function for vibration isolation metamaterial designs. There, the answers on what will be optimized and what the boundary conditions are will be provided. The second part provides several commonly used optimization methods with their respective benefits and negative aspects. In addition, the second part introduces several normalized characteristics that can be used to compare these optimization methods. The final part provides a comparison table that shows each discussed method with specific characteristics from the second part. This table is designed

to help choose an optimization method for the specific study case of a vibration isolation metamaterial.

A. Objective function and boundary conditions

Before a design can be optimized, certain aspects need to be defined. Two important aspects of optimization are the objective function, which answers the question of what we are optimizing for, and the boundary conditions.
Firstly, the objective function will be defined. The objective function is a function that will be minimized. Within this function, multiple variables can be changed. Each variable has a unique boundary condition, where the variable cannot cross the boundary condition.
Now to refer back to the case of QZS, we focus on the force-displacement diagram. In this diagram the QZS region is the region where there is a free displacement for a given force, the horizontal curve. There are two objectives in this specific case; the first objective is to minimize the error in the horizontal curve (keeping the curve as horizontal as possible) and the second objective is to maximize the length of the curve where it is horizontal (increasing the size of the QZS region). [8]
The variables will depend on the model. This can vary widely from material properties in specific elements to the number, location and orientation of elements in the model. Each variable has restrictions (boundary conditions) such as a limited element length.
A general problem with optimization methods is that the obtained minimum could be a local minimum instead of a global minimum. That means that there may exist a more optimal solution than the one that was found. Some algorithms are more robust in finding the global minimum than others. There are certain methods to check if a minimum is local or global, and there are certain methods to help the algorithm in finding the global minimum instead of a local minimum.[22]
One aspect, which has the most influence on finding the global minimum, is the initial state (starting structure). Based on the starting structure the algorithm searches for the minimum. Choosing the starting structure wisely forces the algorithm to start searching closer to the global minimum. Additionally, this will also decrease computational costs as the algorithm reaches the global minimum much faster.[22], [23]

B. Methods

In the engineering world, there are many optimization methods for different scenarios. This section will only discuss the methods applicable to optimizing a QZS metamaterial. Therefore, not all optimization methods are covered, but only a small selection that is used in similar projects. This selection balances efficiency, adaptability, and computational feasibility, ensuring a robust optimization framework for QZS metamaterials. For each optimization method the most important pros and cons will be discussed. In addition, the performance in several characteristics is graded to help compare these results.

The first characteristic is the cost. The cost of an optimization method is measured in the number of computations necessary to obtain the desired optimum. It must be noted that the number of computations necessary is highly dependent on the initial state, therefore, in this report the average computational cost of the method is assumed.
The second characteristic is how robust an optimization method is. Optimization methods that find good solutions under varying conditions can be labeled as having good robustness.
The third characteristic is related to the precision of the solutions found. High-accuracy optimization methods find the optimal or near-optimal solution, whereas low-accuracy optimization methods find solutions further away from the optimal solution.
Stability is another characteristic of optimization methods that is important to account for. It is essential that when the optimization procedure is run multiple times, the same results are obtained.
The final characteristic is reliability. The optimization procedure can stumble upon a local minimum or a global minimum. Some procedures are more prone to obtain local minima compared to others and are very dependent on the initial state.

Size optimization
Size optimization is the procedure of optimizing the dimensions of a structure. Therefore, the shape of the structure remains the same. The most common methods within this branch are the Quasi-Newton method and gradient search. During this procedure the gradient is used to find the minimum of the objective.[24]–[26]
Size optimization can be very useful as it converges very fast. In addition, due to its simplicity, it is very easy to adjust or add boundary conditions to the system making it flexible. However, size optimization methods are very sensitive to the initial input. Therefore, it is prone to obtain local minima.
Size optimization has low computational costs and is moderately robust as it is less sensitive to uncertainties compared to other more flexible methods like shape optimization. However, this method has worse performance with uncertainties. The solutions found with size optimization can be very accurate due to the precision of the variables and the mathematical model. This method is established from a mathematical framework, which invites a very high precision and a very stable system. However, size optimization is very dependent on the initial state and is therefore very unreliable.[7], [16], [22]–[24], [26], [27]

Shape optimization
Shape optimization is the procedure to find minima or maxima for a specific objective function where the design variables are coordinates or other parameters

that define the shape of a structure. Common methods use FEA computational techniques that require lots of computational resources.
Using shape optimization techniques often results in a better optimum compared to size optimization due to the freedom to reshape the design. In addition, shape optimization requires little prior knowledge as it is less dependent on the initial state. However, it requires complex modeling which is very expensive.
Shape optimization has a high cost. The number of iterations is relatively low, however, every iteration is expensive. This optimization method is slightly robust due to it obtaining consistent good performance under varying conditions, however when dealing with nonlinearity the chances of getting stuck are larger. The main reason for this is that the FEA approach is very robust. For the same reason, the accuracy is also very good. The FEA approach can be very precise, resulting in very accurate optima. Both the stability and the reliability are also very high because this method is not prone to result in local minima and provides the same result when it is repeatedly run.[22]–[24], [26]

Topology optimization
Topology optimization is the process of optimizing the distribution of material to minimize a specific objective function. This optimization process can be done using density-based methods or evolutionary algorithms.
Topology optimization techniques can be very useful when prior knowledge is limited or when innovative solutions are preferred. However, using this method does require a lot of computational resources due to the complexity of the optimization process. In most cases the resultant structure is very difficult to manufacture, requiring a manufacturing check to be performed.
Topology optimization has high costs due to the complex optimization process. However, this is compensated by the high robustness due to obtaining consistent good results under varying conditions. The accuracy of topology optimization is very dependent on the model precision making it either very precise or lacking a certain precision. Topology optimization is moderately stable and moderately reliable because it is sensitive to the initial conditions.[14], [19], [22]–[24]

Genetic optimization
During the genetic optimization process the system produces multiple approximate solutions, followed by a selection of the best and elimination of the worst. Based on this new selection a new set of approximate solutions are produced. After a predefined number of iterations, the best solution is found. Genetic optimization is very useful in always finding good solutions as it performs a global search, after which it starts to search more precisely. Due to this approach the local minima are mostly avoided, thus, having a good reliability. However, this optimization process is very expensive due to the many iterations and calculations necessary to obtain a result. In addition, parameters such as population size and crossover rate can be difficult to properly tune. Genetic optimization provides a high robustness as it obtains good solutions under varying conditions. The accuracy of this optimization technique is moderate as it is not always possible to find the exact optimum within a certain number of generations and the convergence speed is very slow near the optimum. However, a very good accuracy can be obtained if the parameters are perfectly chosen. Therefore, the overall accuracy of this method is moderate. The stability of genetic optimization is moderate due to the dependency on initial conditions and the number of generations. [13], [17], [19], [21]–[24], [28]

C. Comparison table

In this section a comparison table will be proposed. This comparison table will provide the information necessary to choose an optimization method for optimizing a QZS metamaterial. A grade is provided for each characteristic per optimization method. The "+" represents a positive grade, the "0" represents a neutral grade and the "-" represents a negative grade. For example, low costs are preferred and therefore a method with low costs is graded with a "+".

Table II: Optimization comparison table

	Cost	Robustness	Accuracy	Stability	Reliability
Size	+	0	+	+	-
Shape	-	0	+	+	+
Topology	-	+	0	0	0
Genetic	-	+	0	0	+

VI. Discussion

The characterization of the QZS design approaches provides an overview of the importance within these designs. The buckling approach proves only to be applicable for low forces. Therefore, a design consisting of a positive and negative stiffness element is ideal for the purpose of QZS metamaterial because of greater design freedom.
The beam-node network modelling method may be less accurate compared to a FEM analysis, therefore, a good accurate validation method is beneficial. One step to obtain a more accurate result is to use dogbone specimen to obtain material properties. To properly verify the analytical results two tests can be done. Firstly, a compressions test must be done, resulting in a force-displacement diagram (or stress-strain) which should show the QZS region and its corresponding force. Secondly, a vibration test can be performed using three masses (before QZS zone, within QZS zone, and after QZS zone). Note that the vibration test is only applicable after the QZS zone is obtained through the compression test.

The beam-node network model can act as a good approach for optimization of QZS metamaterial. The proposed model from Prasad [19] and Jang [21] provides a good approach for modelling the joints, where the stiffness can be adjusted through variables such as cross-sectional

area and material property. The proposed model divides the beams into three sections, with the outer sections representing the joints. Each section is assigned distinct material properties and cross-sectional areas to facilitate joint rotation.
Additional complexity can be added to the model by implementing parameters proposed in the paper by Sauter [13]. These parameters describe variable thicknesses of the beams and curvatures in the beams. However, these additional parameters should only be implemented to increase complexity if required.
The spanning tree method is a good approach to obtain a full design within prescribed boundaries, including optimization.[15] However, this does require additional steps to obtain a manufacturable design, such as a threshold limit removal phase and a graph based element search and cut phase.[14]
Converting the model to a physical design might prove to be difficult, as many papers only compared the model to a FEM simulation or other existing designs instead of directly comparing to a physical design. The best solution for now is to convert the obtained design to a FEM model using a smoothing process. Based on that FEM model a physical design can be manufactured.
As discussed in the optimization section, the focus of this literature review is on assessing methods for maximizing the QZS region in the force-displacement curve. A selection of four optimization methods is further explained and compared to five important aspects, resulting in a comparison table (Table II). According to the comparison table both size and shape optimization are good options. However, it must be mentioned that genetic optimization is a close third, with the potential to be the best option if the optimization parameters are properly tuned.

VII. Conclusion

In this literature review, a solid background for the design and optimization of a vibration isolation metamaterial is presented. The design method is divided into three segments; the QZS design approach, how the design can be modelled, and the applicable optimization methods.

The model is used in this literature review is a set of beams connected by ball-joints (nodes). In this specific model the emphasis is placed on having few elements to reduce calculation costs. The most notable variables within a beam-node network model are the length of the beams, the cross-sectional area of the beams, and the material property of the beams. Additional variables, such as variable thickness and curved beams, can be used to increase complexity.

The quasi-zero stiffness (QZS) approach is widely employed in the design of vibration isolation metamaterials. Two primary design strategies are discussed in the literature review. The first approach involves the combination of positive stiffness (PS) elements and negative stiffness (NS) elements to achieve the QZS property through an effective stiffness balance. The second approach leverages structural buckling, wherein pre-compressed or post-buckled elements introduce a near-zero stiffness region. Each of these approaches offers distinct advantages and limitations, which are further analyzed in subsequent sections.
The validation of the QZS property can be achieved by performing a compression test, resulting in a force-displacement diagram. Within this force-displacement diagram a QZS region can be seen. A second test can be performed by using a shaker with specific masses that correspond to the force of the force-displacement diagram. From the resultant transmittance-frequency graph a negative transmittance indicates the QZS property.

The optimization process of a QZS metamaterial requires the objective function to have two parts in the force-displacement curve. The first part is to maximize the size of the QZS region. The second part is to minimize the force deviation within this region. Four optimization methods (size, shape, topology, and genetic optimization) are discussed and compared to five characteristics (cost, robustness, accuracy, stability, and reliability), resulting in a comparison table.

This review provides a comprehensive foundation for the design, modelling, and optimization of QZS-based vibration isolation metamaterials.

REFERENCES

[1] H. Fan, L. Yang, Y. Tian, and Z. Wang, "Design of metastructures with quasi-zero dynamic stiffness for vibration isolation," *Composite Structures*, vol. 243, Jul. 2020, ISSN: 02638223. DOI: 10.1016/j.compstruct.2020.112244.

[2] J. Liu, Y. Wang, S. Yang, T. Sun, M. Yang, and W. Niu, "Customized quasi-zero-stiffness metamaterials for ultra-low frequency broadband vibration isolation," *International Journal of Mechanical Sciences*, vol. 269, May 2024, ISSN: 00207403. DOI: 10.1016/j.ijmecsci.2024.108958.

[3] S. Guo, R. Gao, X. Tian, and S. Liu, "A quasi-zero-stiffness elastic metamaterial for energy absorption and shock attenuation," *Engineering Structures*, vol. 280, Apr. 2023, ISSN: 18737323. DOI: 10.1016/j.engstruct.2023.115687.

[4] S. Guo, S. Liu, and R. Gao, "A bidirectional quasi-zero stiffness metamaterial for impact attenuation," *International Journal of Mechanical Sciences*, vol. 268, Apr. 2024, ISSN: 00207403. DOI: 10.1016/j.ijmecsci.2024.108998.

[5] Y. Zheng, W. B. Shangguan, Z. Yin, and X. A. Liu, "Design and modeling of a quasi-zero stiffness isolator for different loads," *Mechanical Systems and Signal Processing*, vol. 188, Apr. 2023, ISSN: 10961216. DOI: 10.1016/j.ymssp.2022.110017.

[6] K. Liang, Y. Jing, and X. Zhang, "Design of broad quasi-zero stiffness platform metamaterials for vibration isolation," *International Journal of Mechanical Sciences*, vol. 281, Nov. 2024, ISSN: 00207403. DOI: 10.1016/j.ijmecsci.2024.109691.

[7] Q. Zhang, D. Guo, and G. Hu, "Tailored Mechanical Metamaterials with Programmable Quasi-Zero-Stiffness Features for Full-Band Vibration Isolation," *Advanced Functional Materials*, vol. 31, no. 33, Aug. 2021, ISSN: 16163028. DOI: 10.1002/adfm.202101428.

[8] Y. Xu, H. W. Dong, and Y. S. Wang, "Topology optimization of programable quasi-zero-stiffness metastructures for low-frequency vibration isolation," *International Journal of Mechanical Sciences*, vol. 280, Oct. 2024, ISSN: 00207403. DOI: 10.1016/j.ijmecsci.2024.109557.

[9] R. Hamzehei, M. Bodaghi, and N. Wu, *Mastering the art of designing mechanical metamaterials with quasi-zero stiffness for passive vibration isolation: a review*, Aug. 2024. DOI: 10.1088/1361-665X/ad5bcc.

[10] B. Ding, X. Li, S. C. Chen, and Y. Li, "Modular quasi-zero-stiffness isolator based on compliant constant-force mechanisms for low-frequency vibration isolation," *JVC/Journal of Vibration and Control*, vol. 30, no. 13-14, pp. 3006–3020, Jul. 2024, ISSN: 17412986. DOI: 10.1177/10775463231188160.

[11] Y. Chen, "3D Texture Mapping for Rapid Manufacturing," Tech. Rep. 6, 2007, pp. 761–771. [Online]. Available: www.ptc.com.

[12] P. J. Bradley, "A multi-fidelity based adaptive sampling optimisation approach for the rapid design of double-negative metamaterials," Tech. Rep., 2013, pp. 87–114.

[13] M. Sauter, G. Kress, M. Giger, and P. Ermanni, "Complex-shaped beam element and graph-based optimization of compliant mechanisms," *Structural and Multidisciplinary Optimization*, vol. 36, no. 4, pp. 429–442, Oct. 2008, ISSN: 1615147X. DOI: 10.1007/s00158-007-0182-7.

[14] F. Danzi, J. M. Gibert, G. Frulla, and E. Cestino, "Graph-based element removal method for topology synthesis of beam based ground structures," *Structural and Multidisciplinary Optimization*, vol. 57, no. 4, pp. 1809–1813, Apr. 2018, ISSN: 16151488. DOI: 10.1007/s00158-017-1818-x.

[15] H. Zhou and K.-L. Ting, "Topological Synthesis of Compliant Mechanisms Using Spanning Tree Theory," *Journal of Mechanical Design - J MECH DESIGN*, vol. 127, Jul. 2005. DOI: 10.1115/1.1900148.

[16] C. C. Lan, "Analysis of large-displacement compliant mechanisms using an incremental linearization approach," *Mechanism and Machine Theory*, vol. 43, no. 5, pp. 641–658, May 2008, ISSN: 0094114X. DOI: 10.1016/j.mechmachtheory.2007.03.010.

[17] P. V. Hull, M. L. Tinker, and G. Dozier, "Evolutionary optimization of a geometrically refined truss," *Structural and Multidisciplinary Optimization*, vol. 31, no. 4, pp. 311–319, Apr. 2006, ISSN: 1615147X. DOI: 10.1007/s00158-005-0564-7.

[18] V. S. Deshpande, M. F. Ashby, and N. A. Fleck, "Foam topology bending versus stretching dominated architectures," Tech. Rep., 2001, pp. 1035–1040. [Online]. Available: www.elsevier.com/locate/actamat.

[19] J. Prasad and A. R. Diaz, "Synthesis of bistable periodic structures using topology optimization and a genetic algorithm," *Journal of Mechanical Design*, vol. 128, no. 6, pp. 1298–1306, 2006, ISSN: 10500472. DOI: 10.1115/1.2338576.

[20] M. A. Crisfield, "Non-linear Finite Element Analysis of Solids and Structures," Tech. Rep., May 2000.

[21] G. W. Jang, M. J. Kim, and Y. Y. Kim, "Design optimization of compliant mechanisms consisting of standardized elements," *Journal of Mechanical Design*, vol. 131, no. 12, pp. 1 210 061–1 210 068, 2009, ISSN: 10500472. DOI: 10.1115/1.4000531.

[22] P. Y. Papalambros and D. J. Wilde, *Principles of optimal design : modeling and computation*. Cambridge University Press, 2000, p. 390, ISBN: 0521622158.

[23] A. R. Parkinson, R. J. Balling, and J. D. Hedengren, "Optimization Methods for Engineering Design Applications and Theory," Tech. Rep., 2013.

[24] A. D. Belegundu and T. R. Chandrupatla, "Optimization Concepts and Applications in Engineering," 2019.

[25] J. Zhou, H. Pan, C. Cai, and D. Xu, "Tunable ultralow frequency wave attenuations in one-dimensional quasi-zero-stiffness metamaterial," *International Journal of Mechanics and Materials in Design*, vol. 17, no. 2, pp. 285–300, Jun. 2021, ISSN: 15738841. DOI: 10.1007/s10999-020-09525-7.

[26] J. Joo, S. Kota, and N. Kikuchi, "Topological synthesis of compliant mechanisms using linear beam elements," *Mechanics of Structures and Machines*, vol. 28, no. 4, pp. 245–280, Nov. 2000, ISSN: 08905452. DOI: 10.1081/SME-100102022.

[27] Z. Satterfield, N. Kulkarni, G. Fadel, G. Li, N. Coutris, and M. P. Castanier, "Unit cell synthesis for design of materials with targeted nonlinear deformation response," *Journal of Mechanical Design*, vol. 139, no. 12, Dec. 2017, ISSN: 10500472. DOI: 10.1115/1.4037894.

[28] Y. Li, X. Huang, Y. M. Xie, and S. W. Zhou, "Evolutionary topology optimization of hinge-free compliant mechanisms," *International Journal of Mechanical Sciences*, vol. 86, pp. 69–75, 2014, ISSN: 00207403. DOI: 10.1016/j.ijmecsci.2013.10.013.